Optical properties of one-dimensional semiconductors

Franz-Keldysh and excitonic effects

Bonabi, Farzad

Publication date:
2019

Document Version
Publisher's PDF, also known as Version of record

Link to publication from Aalborg University

Citation for published version (APA):
Bonabi, F. (2019). *Optical properties of one-dimensional semiconductors: Franz-Keldysh and excitonic effects*. Aalborg Universitetsforlag.

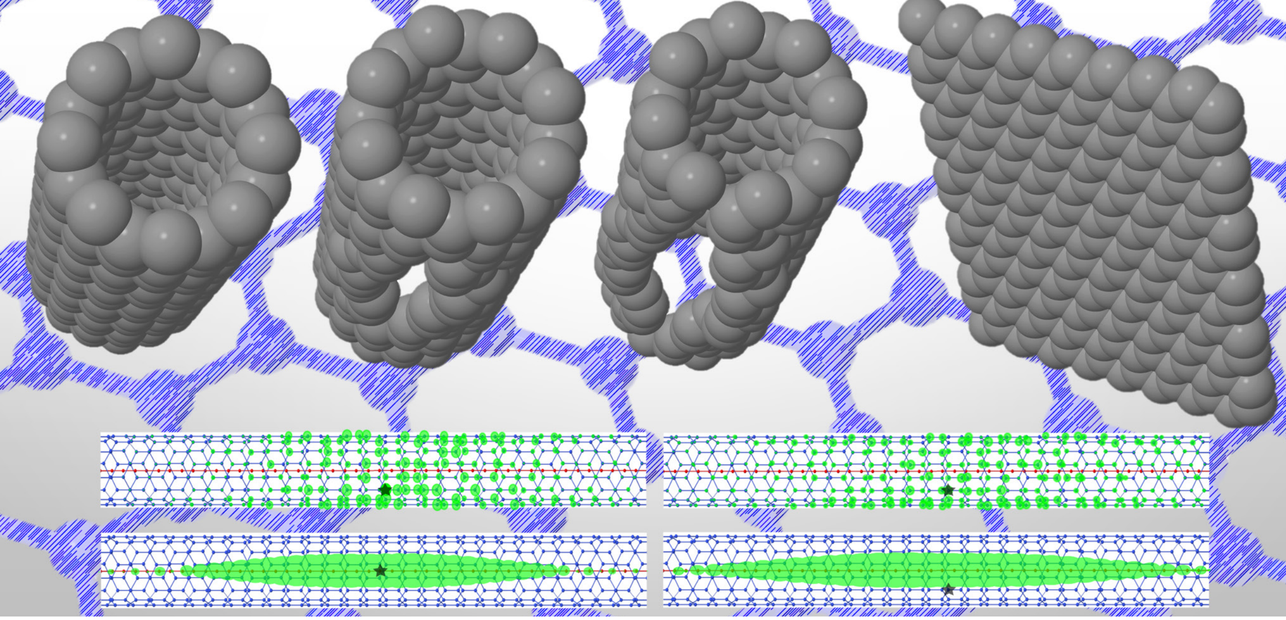

OPTICAL PROPERTIES OF ONE-DIMENSIONAL SEMICONDUCTORS

FRANZ-KELDYSH AND EXCITONIC EFFECTS

BY
FARZAD BONABI

DISSERTATION SUBMITTED 2019

AALBORG UNIVERSITY
DENMARK

Optical properties of one-dimensional semiconductors

Franz-Keldysh and excitonic effects

Ph.D. Dissertation

Farzad Bonabi
Department of Materials and Production
Aalborg University

AALBORG UNIVERSITY
DENMARK

Dissertation submitted February, 2019

Dissertation submitted: February, 2019

PhD supervisor: Prof. Thomas Garm Pedersen
Aalborg University

PhD committee: Associate Professor Lars Diekhöner (chairman)
Aalborg University

Professor, Dr. Techn, N. Asger Mortensen
University of Southern Denmark

Dr. habil. Sergey A. Mikhailov
University of Augsburg

PhD Series: Faculty of Engineering and Science, Aalborg University

Department: Department of Materials and Production

ISSN (online): 2446-1636
ISBN (online): 978-87-7210-402-7

Published by:
Aalborg University Press
Langagervej 2
DK – 9220 Aalborg Ø
Phone: +45 99407140
aauf@forlag.aau.dk
forlag.aau.dk

Printed in Denmark by Rosendahls, 2019

Abstract

The main focus of this thesis is to calculate the electronic structure and optical response of one-dimensional semiconductors with and without many-body excitonic effects and the presence of strong external electrostatic fields. To investigate these effects, several quasi-one-dimensional semiconductors such as carbon nanotubes (CNTs) and chains, which are important materials in electrical and optical applications.

It is widely known that electron-hole interactions considerably influence the charge distribution and optical properties of one-dimensional semiconductors. Recent studies have shown that long carbyne systems can be grown inside CNTs and new hybrid CNT-carbyne systems are formed, which their electronic structure, as well as the single-electron and excitonic optical response, are expected to differ considerably with those of isolated CNT and carbyne systems. CNTs and carbyne systems interact with each other via the long-range Coulomb interaction. There are direct excitons, which electrons and holes are on either CNT or carbyne systems, as well as spatially indirect excitons, where electrons are on CNT and holes are located on carbyne systems or vice versa. In this thesis, we investigate the electronic structure of CNT-carbyne systems using a tight-binding calculation fitted against a density functional-based band structure. Then, the exciton binding energy for above-mentioned exciton types and the excitonic optical response of these hybrid systems are calculated using the Bethe-Salpeter and Wannier methods. Alongside excitons on each subsystem in the hybrid structure, interactions between two subsystems result in new bright excitons. Also, such interactions cause charge-transfer dark excitons, which are indirect excitons.

Static electric fields considerably modify the electronic structure and optical response of semiconductors. These fields in the periodic direction of one-dimensional semiconductors tilt the potential and break the periodicity, and transform energy band structure to a localized set of energy states known as the Wannier-Stark ladder. In this thesis, we present an approach for studying the effect of static electric fields in two- and multiband models of one-dimensional semiconductors and compare finite and infinite length results. For infinite length, a novel density matrix method is developed in reciprocal space for calculating the non-perturbative Franz-Keldysh effect, which is computationally much faster than the quantum perturbation method for finite systems. This infinite method is applied for infinite polyacetylene and graphene nanoribbons with various widths and results are compared with those of finite systems. Moreover, field-induced second-order nonlinear optical response due to the broken center of symmetry for these systems is studied for both finite and infinite lengths. Furthermore, the method is extended for two-dimensional semiconductors and convergence of graphene nanoribbons optical response to that of the two-dimensional graphene is investigated. For graphene nanoribbons, we also apply DC fields along the perpendicular direction of the infinite direction in these systems and calculate the electronic structure and optical response.

Resumé

Det primære fokus i denne tese er at udregne den elektroniske stuktur og optisk respons af endimensionelle halvledere både med og uden many-body eksitoniske effekter samt under indflydelse af stærke eksterne elektrostatiske felter. For at undersøge disse effekter, betragtes flere kvasi-endimensionelle halvledere, såsom kulstof-nanorør og -kæder, som er vigtige materialer med elektroniske og optiske anvendelsesmuligheder.

Det er alment kendt at elektron-hul interaktioner har betragtelig indflydelse på ladningsfordelingen og optiske egenskaber af endimensionelle halvledere. Nye studier har vist at lange carbyn-systemer kan syntetiseres inde i kulstof-nanorør, hvorved nye hybrid nanorør-carbyn-systemer dannes, som forventes at have signifikant anderledes elektronisk og optisk respons i forhold til de isolerede nanorør og carbyn-systemer. Nanorør og carbyn systemer interagerer med hinanden via en langtrækkende Coulombinteraktion. Der er direkte eksitoner, hvor både elektronen og hullet forefindes enten på nanorøret eller carbynet, samt rummeligt indirekte eksitoner, hvor elektronen findes på nanorøret og huller på carbynet og omvendt. I denne tese undersøges den elektroniske struktur af nanorør-carbyn-systemer ved brug af tight-binding udregninger, der er fittet til en båndstruktur udregnet med tæthedsfunktionalteori (DFT). Derefter beregnes den eksitoniske bindingsenergi og eksitonisk optisk respons for førnævnte eksiterings-typer ved brug af Bethe-Salpeter og Wannier metoderne. Sammen med eksitoner på hvert undersystem i hybridstrukturen, forsager interaktionen mellem systemerne nye lysende eksitoner. Derudover forsager interaktionen ladningsoverførsels-eksitoner, der er indirekte eksitoner.

Statiske elektriske felter ændrer markant på den elektroniske struktur og optiske respons for halvledere. Når feltet peger langs den periodiske retning af endimensionelle halvledere, tiltes potentialet og periodiciteten brydes, og transformerer båndstrukturen til et lokaliseret set af energitilstande, også kendt som en Wannier-Stark ladder. I denne tese præsenteres en fremgangsmåde for at studere effekten af statiske elektriske felter i to- og multibånd modeller af endimensionelle halvledere, samt sammenligner resultater for endeligt og uendeligt lange strukturer. For uendeligt lange strukturer udvikles en ny tæthedsmatriksmetode i reciprokt rum for at udregne de ikke-pertuberede Franz-Keldysh effekt. Denne metode er beregningsmæssigt meget hurtigere end kvanteperturberingsmetoden for endelige systemer. Denne metode for uendelige systemer benyttes til polyacetylen og grafen nanoribbons med forskellige bredder og resultaterne sammenlignes med resultater for endelige systemer. Derudover studeres det felt-inducerede anden-ordens ikke-linære optiske respons, der forekommer grundet den brudte centersymmetri for disse systemer. Metoden udvides til todimensionelle halvledere og konvergensen af det optiske respons for grafen nanoribbons sammenlignes med todimensionelt grafen. For grafen nanoribbons påføres også et DC elektrisk felt vinkelret på nanoribbon planet og den tilhørende elektriske struktur og optiske respons beregnes.

Contents

Abstract iii

Resumé v

Thesis Details ix

Preface xi

1 Introduction 1
- 1.1 This thesis 9

2 Theory and Methods 13
- 2.1 Electronic structure 13
  - 2.1.1 Density functional theory 13
  - 2.1.2 Tight-binding method 14
- 2.2 Single-electron optical response 15
  - 2.2.1 Finite system 17
  - 2.2.2 Infinite system 19
- 2.3 Exciton states 21
  - 2.3.1 Bethe-Salpeter equation 21
  - 2.3.2 Wannier approximation 22
  - 2.3.3 Excitonic optical response 23
- 2.4 Static electric field and Franz-Keldysh effect 24
  - 2.4.1 Transversal DC fields 24
  - 2.4.2 Longitudinal DC fields 25
  - 2.4.3 Two-dimensional semiconductors 29

3 Summary of results 31
- 3.1 Electronic structure 31
  - 3.1.1 Hybrid CNT-carbyne systems 31
  - 3.1.2 Graphene nanoribbons in transversal DC fields 33
- 3.2 Independent-electron optical response 35

3.2.1 One-dimensional carbon-based atomic chains 35
3.2.2 CNT-carbyne systems 36
3.2.3 Graphene nanoribbons and sheet 37
3.3 Excitonic effects in CNT-carbyne systems 39
3.4 Transversal DC fields in graphene nanoribbons 44
3.5 Longitudinal DC fields in Semiconductors 45
3.5.1 Polyacetylene chains 46
3.5.2 Narrow graphene nanoribbons 47
3.5.3 Wide AGNRs and graphene sheet 50

4 Conclusions **53**
. . . . 57

Thesis Details

Thesis title:	Optical properties of one-dimensional semiconductors: Franz-Keldysh and excitonic effects
Ph.D. student:	Farzad Bonabi
Supervisor:	Thomas Garm Pedersen

The main body of this thesis consists of the following papers:

[**I**]. **F. Bonabi** and T. G. Pedersen, “Linear and nonlinear optical response of one-dimensional semiconductors: finite-size and Franz–Keldysh effects”, J. Phys.: Condens. Matter. **29**, 165702 (2017).

[**II**]. **F. Bonabi**, S. J. Brun, and T. G. Pedersen, “Excitonic optical response of carbon chains confined in single-walled carbon nanotubes”, Phys. Rev. B **96**, 155419 (2017).

[**III**]. **F. Bonabi** and T. G. Pedersen, “Franz-Keldysh effect and electric field-induced second harmonic generation in graphene: From one-dimensional nanoribbons to two-dimensional sheet”, Phys. Rev. B **99**, 045413 (2019).

This thesis has been submitted for assessment in partial fulfillment of the Ph.D. degree. The thesis is based on the published scientific papers which are listed above. Parts of the papers are used directly or indirectly in the summary in the thesis. As part of the assessment, co-author statements have been made available to the assessment committee and are also available at the Faculty. The thesis is not in its present form acceptable for open publication but only in limited and closed circulation as copyright may not be ensured.

Preface

This thesis summarizes my research program as a PhD student at the Department of Materials and Production (former Department of Physics and Nanotechnology), Aalborg University, in the past four years in the period 2015-2019, under the supervision of Professor Thomas Garm Pedersen. This PhD program was part of the QUSCOPE research project founded by Villum Foundation.

Moving to Denmark in January 2015 to experience living abroad as a PhD student and start a challenging and enjoyable research program in condensed matter physics and theoretical quantum optics was the most important decision in my life. I am happy that I could fulfill this step with great achievements. There are several people who have helped and supported me to start and finish this PhD program. First and foremost, I would like to gratefully thank Thomas Garm Pedersen who offered this exciting position at his research group and has continuously supported me during my research. He is very skilled and talented, not only as a teacher and scientist but also in the wild-life photography and fishing. I recommend everyone to check out his website for amazing wild-life pictures. I would also like to thank Mads Lund Trolle. I never forget that you picked me up from Aalborg Airport when I arrived Aalborg for the first time and your helpful discussions in my research projects as well as the great atmosphere in the office. I would like to thank Kristian Bonderup Pedersen, Alireza Taghizadeh and Fábio Hipólito for their great company in the office and occasional events we were together. I would like to thank René Petersen for inviting me to his amazing wedding in Madrid and also his great company in NANOP Conference 2016 in Paris, Morten Rishøj Thomsen for his always welcoming attitude and smiley face in helping occasional programming problems, and Søren Jacob Brun for his company in the fitness and hanging out plans. I would like to thank Mads Brincker for his help in passing through the procedure of buying a computer and accessories for work and my home furniture from IKEA. I would also like to thank Jonas Have for joining in the refreshing table tennis matches at the basement and also watching Game of Thrones episodes when we needed a break from extensive coding. I wish to have special thanks to my parents and siblings for their support during my PhD. Last, but not least, I would like to thank my fiancé Pegah Bagheri Biglari for her great support and encouragements, especially in my very absent-minded moments during my PhD.

Farzad Bonabi
Aalborg University, February 27, 2019

Chapter 1

Introduction

The atomic structure (the arrangement of atoms in a material) has a significant role in the physical properties of that material. For instance, while diamond and graphite are both constructed by carbon atoms, they are two different materials because of their different physical properties. Diamond is an insulator and very hard material [1], whereas graphite is a semimetal and its hardness is much smaller than diamond [2]. In solid state physics, crystal structures are usually categorized by Bravais lattices, in which the physical properties of each lattice could be different from other lattices. Several parameters such as atomic bond lengths, angles between atomic bonds and also dimensionality of systems are responsible in differentiating lattices. In the mentioned example, diamond is a two inter-penetrated face-centered cubic (FCC) lattices [3], and graphite is an infinite stack of two-dimensional hexagonal lattices with a two-atomic basis. Thus, defining the atomic structure is the initial step in the theoretical study of any material.

Among the mentioned geometrical parameters in the atomic structure of a lattice, the dimension has crucial importance in defining the physical properties of that lattice. In the above-mentioned example, graphite is a three-dimensional structure. If one can isolate only one layer of the graphite honeycomb stack, the resulting structure is graphene [4]. Graphene is also a semimetal, but its reduced dimensionality causes different physical properties compared to graphite such as high electron mobility [5]. In general, confining charge carriers in one or more dimensions changes the physical properties of atomic systems. If the confinement is in one dimension, systems are two-dimensional like graphene. Two- and three-dimensional confinements lead to one-dimensional materials like nanowires [6, 7] and quantum dots [8], respectively.

The main focus of this thesis is investigating the optical response of one-dimensional semiconductors. Hence, before discussing the effect of reducing the dimensionality on the optical response, the following question should be answered: What is the optical response? Optical properties of materials are, in fact, the result of the interaction of those materials with external electromagnetic fields (light). In optical processes, the electric part of external light is considered to interact with the system by inducing the polarization. As results, absorption, emission, refraction of light or combinations of them can occur in the system. These phenomena are the optical response of materials to the external light. The optical response of different types of material are different. If a material is an insulator, the optical field induces local dipoles in the system. For conductors, the external light generates inductive currents, due to the displacement of charges. In semiconductors, Light can induce dipole moments and be absorbed when the photon energy is larger than the band gap energy of the system. The optical response of semiconductors depends not only on the optical band gap, but also impurities, temperature, electron-hole interactions, electron-phonon couplings, etc. The band gap of a semiconductor has crucial importance in the optical response because it defines the minimum energy that optical photons must possess to interact with the system. Studying the optical band gap and optical response of semiconductors has practical importance because many optical devices such as optical diodes [9], solar cells [10] and diode lasers [11] are based on the optical properties of semiconductors.

Light does not always interact linearly with a material. An experiment by Franken et al. in 1961 resulted in finding the second harmonic generation (SHG) in quartz [12], which was a nonlinear process. This experiment has attracted a lot of attention to the nonlinear optical response of materials. Sufficiently strong external optical fields are necessary to get a noticeable nonlinear optical response from a system. Nonlinear optics has a broad range of applications such as a tool for material characterization [13] and optoelectronics [14].

Studying lower-dimensional semiconductors leads to finding new materials with remarkable potential in various electrical and optical applications. Reducing the dimensionality of a semiconductor causes modifications in the electronic structure and the band gap energy, and results in significant changes in the optical response of the system. For instance, bulk silicon as the most used semiconductor in electrical applications has an indirect band gap [15]. For materials with the indirect band gap in low temperatures, light absorption can be a difficult process, however, reducing the dimensionality can modify the band structure and lead to materials with a direct band gap such as silicon nanoclusters. Because the direct band gap can facilitate light-matter interactions, silicon nanoclusters, which can be treated as quantum dots [16], are good candidates in optical devices [17].

The reduced dimensionality in one-dimensional semiconductors changes the density of states of charge carriers in these materials and results in different optical responses compared to their two- and three-dimensional counterparts [18]. One-dimensional materials can be classified into different groups such as tubes, wires, belts, chains, ribbons, etc. Most of the materials in these groups are

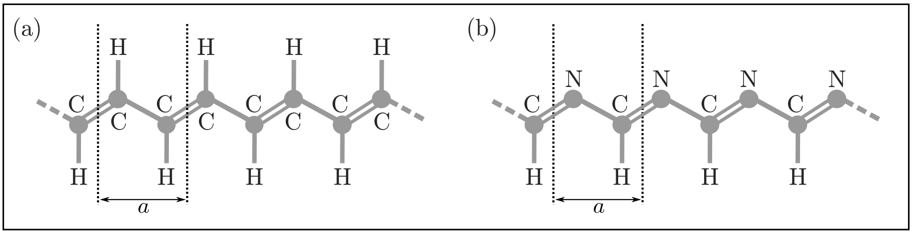

Fig. 1.1: The atomic structure of (a) polyacetylene and (b) polymethineimine. The dashed line with the width of a is the unit cell for each structure.

not, in fact, one-dimensional, i.e., their atomic structure can be two- or three-dimensional, whereas they show one-dimensional behavior because their structure is a repeating unit cell in only one direction. Thus, they are often called quasi-one-dimensional materials. In recent decades, carbon-based semiconductors have attracted a tremendous amount of attention both theoretically and experimentally, due to their outstanding potential in various electrical and optical applications. In the following, studied one-dimensional semiconductors in this thesis are introduced.

Organic carbon-based chains are simple one-dimensional semiconducting structures. Chemical bonds and structure of these materials can be diverse, in which they have interesting electronic and optical features [19, 20]. Polyacetylene and polymethineimine chains in Fig. 1.1 are two examples of semiconducting carbon chains, which their molecular structure are single and double carbon-carbon and nitrogen-carbon bonds, respectively, and their free chemical bonds are passivated by hydrogen atoms.

One-dimensional carbon-based structures can be more complex than simple atomic chains. Carbon nanotubes (CNTs) are one of good examples of quasi-one-dimensional carbon-based structures. These materials are, in fact, graphene sheets that are rolled around a cylinder and can be produced as single- or multi-walled CNTs. The angle of rolling, which is often referred to as the chiral angle, determines the metallic or semiconducting behavior of CNTs [21]. Such CNTs are usually classified with chiral indices (n, m). There are several methods to synthesize CNTs such as chemical vapor depositions [22] and arch-discharge techniques [23]. Multi-walled CNTs can also provide a suitable medium to grow stable long carbon chains such as carbyne [24] because isolated long carbyne chains are not stable one-dimensional materials. Longer carbyne chains (more than 300 carbon atoms) can be synthesized inside double-walled CNTs, in which the inner tubes have the diameter between 0.62-0.85 nm [25]. This encapsulation leads to novel quasi-one-dimensional hybrid CNT-carbyne systems, which their physical properties are expected to have a combination of properties from CNT, carbyne, and interactions between two subsystems. (8,0) and (10,0) CNTs are two semiconducting CNTs that their diameter is

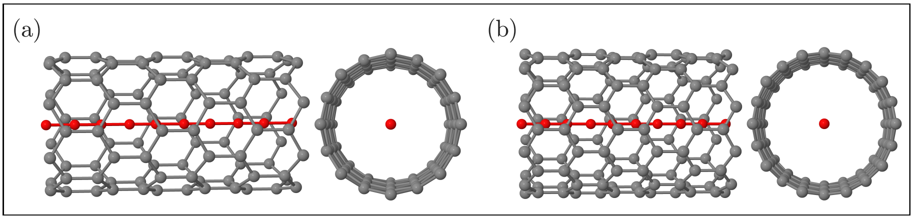

Fig. 1.2: The atomic unit cell of (a) (8,0) CNT-carbyne (b) (10,0) CNT-carbyne, from the side and front views. Gray and red atoms are carbon atoms on CNT and carbyne systems, respectively.

in the range of the optimum CNT diameter to grow long carbyne chains [25]. Figure 1.2 shows a small cut (unit cell) of the atomic structure of (8,0) and (10,0) CNT-carbyne systems from the side and front views.

Graphene nanoribbons (GNRs) are another type of quasi-one-dimensional carbon-based materials, which are studied in this thesis. These structures are two-dimensional graphene sheets, in which they are limited in one direction and infinite atomic units in the other direction. There are several methods to synthesize GNRs such as cutting or unzipping multiwalled CNTs [26, 27]. Moreover, they can be fabricated with high precisions by scanning tunneling microscope (STM) lithography [28] and bottom-up techniques [29]. The width and edge shape are two important geometrical parameters that change the physical properties of GNRs. Armchair-edge GNRs (AGNRs) are semiconductors, while zigzag-edge GNRs (ZGNRs) have metallic properties. Figure 1.3 shows the atomic structure of an AGNR and a ZGNRs limited within hard-walls shown by the red dashed lines along the width direction. The atomic structure and physical properties of both AGNRs and ZGNRs converge to the pristine graphene, provided that they are sufficiently wide. Due to the semiconducting behavior of AGNRs, they will be studied in this thesis. Sufficiently

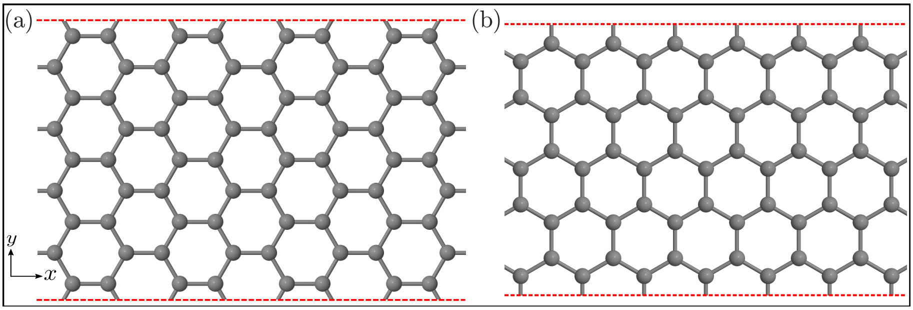

Fig. 1.3: Schematic atomic structure of (a) AGNRs (b) ZGNRs in the x-y plane. The dashed lines are hard-walls, which define the finite width of structures along y-axis. Structures are extended infinitely along x-axis.

wide AGNRs can resemble the properties of the two-dimensional graphene, which for graphene, both x and y directions are extended infinitely.

The first step in the theoretical study of the optical response for the introduced materials is defining the electronic structure of these systems. The reason is that in the atomic scale, electrons are mainly responsible for the optical response. Theoretically, first principal or *ab initio* methods such as density functional theory (DFT) and non-*ab initio* models like the tight-binding (TB) method are commonly used to define the electronic structure and band gap energy of semiconductors. Although the TB model estimates the band structure for these systems with a good accuracy around the band gap energy region, the DFT method is more accurate quantum mechanical approach than TB for obtaining the electronic band structure [30], not only for the band gap region but also for wider energy limits. The DFT method is a self-consisting method using Kohn-Sham equations, which means that there is no need for prior information of the system for calculations. There are two problems in the DFT method: firstly, this method is computationally very demanding, especially for large systems; secondly, it usually underestimates the band gap energy [31]. The reason for the second problem is that the traditional DFT method calculates the ground state of systems. Thus, excited states which are important in defining the band gap energy are not well described in this method. Therefore, this method casts problems in the calculation of the optical response of semiconductors. To solve the band gap energy issue, the GW approximation on top of DFT corrects the excited states and solves the band gap energy problem [32–35]. On the other hand, TB is not computationally costly and capable of obtaining the electronic structure for large systems. The TB method is also referred to as the linear combination of atomic orbitals (LCAO) method because it uses atomic orbitals as the basis for TB wave functions. In contrast with DFT, in the TB method, knowing the orbital basis, as well as overlap and hopping parameters between neighboring sites, are necessary for calculations, for which experimental or first-principal methods data are used to determine these parameters. Moreover, in this approximation, the wave function of electrons are assumed to be localized on atomic sites of semiconductors. Hence, wave functions of each site have overlap with few neighboring sites. In most cases, considering the first nearest neighbor (1NN) for overlapping between sites, provides a satisfactory approximation of the electronic structure compared to DFT in the low energy limit.

For carbon-based conjugated polymers, *ab initio* methods have obtained the band gap energy, in which this energy depends on the structure and constitutional atoms of the polymer [36]. Experimental techniques such as scanning tunneling microscopy have been utilized to find the electronic structure and band gap energy of various single- and multi-walled CNTs and showed that the band gap energy and metallic or semiconducting behavior of CNTs are strongly related to their diameter and helicity (chirality) [37–41]. Moreover, theoretical methods predict similar results for the electronic structure and band gap energy with similar conditions as experiments [42–44]. As mentioned earlier, long carbon chains can be grown inside CNTs. It has been shown that the encapsulation of carbyne inside CNTs results in the interaction between these two systems and reduce carbyne band gap energy [45]. Thus, it is expected that hybrid CNT-carbyne systems show different electronic structure compared to isolated CNT and carbyne systems.

For GNRs, the calculation of the electronic structure using the TB method predicts semiconducting behavior (band gap existence) for type AGNR-($3n_d$) and AGNR-($3n_d + 1$) and metallic behavior for type AGNR-($3n_d + 2$), which n_d is the row number of carbon-carbon bonds along y-direction in Fig. 1.3, and all ZGNRs are metallic [46, 47]. In contrast to TB, first principal calculations predict that all AGNRs and ZGNRs are a semiconductor with a very small band gap energy for type AGNR-($3n_d + 2$) and ZGNRs [48, 49]. Experimentally, the semiconducting behavior of all types of GNRs is observable [50]. All of these studies, as well as Ref. [51] have shown that the electronic structure and physical properties of GNRs are strongly related to the width and edge shape of these systems. With increasing the width of GNR, the band gap shrinks and a graphene-like behavior is expected.

The optical response of materials can be calculated theoretically using their electronic structure. For various conjugated polymers, absorption spectra have been numerically calculated and compared to experimental data [52]. For GNRs, the linear optical response of various AGNRs and ZGNRs, as well as plasmonic effects are calculated theoretically [53–58]. Results show that the optical response and plasmonic effects of GNRs depends on the edge shape and width of these structures. Narrow AGNRs show considerable optical photons absorption with the energy of the band gap. Increasing the width reduces the band gap energy and changes the band structure of GNRs. Moreover, experimental measurements of GNRs optical response have shown agreements with theoretical results [59]. For graphene sheets, the linear and nonlinear optical response has been calculated [60, 61]. Graphene has shown strong third-order nonlinear optical in experimental measurements [62]. For CNTs with various diameters and chiralities, the DFT and TB methods have been utilized to obtain the electronic structure and the linear optical response for optical fields along and parallel to the long-axis of CNT [63, 64]. These studies have shown that the electronic structure and optical response of CNTs depend strongly on the structural characteristics of CNTs. Moreover, absorption spectra have been measured experimentally for various CNTs and shown that the diameter is a very important factor in the optical response of these materials [65].

Theoretical calculations of the optical response in these studies sometimes fail to predict accurately experimental measurements. The reason is that even in the most accurate way of obtaining the band structure, i.e., DFT+GW, the Coulomb interaction between electrons in excited states and holes (lack of electrons) in ground states are not considered in these approximations. The contribution of electron-hole interactions introduces excited states for electrons, which often referred to as excitons. Such excitons are chargeless quasiparticles [66] similar to hydrogen atoms that electrons and holes bound together by Coulomb attractions. The exciton binding energy depends on constitutional atoms and the dimension of the system, as well as surrounding materials. All these factors contribute in the dielectric constant and cause a screening in the Coulomb potential, and result in the reduction of the binding energy. In three-dimensional crystals such as bulk silicon, the lattice screening is large, and the exciton binding energy is a few meV, however, including excitonic effects in the optical response leads to better agreement with experimental data [67]. In the lower-dimensional materials such as quasi-one-dimensional semiconductors, the imposed screening by the structure decreases because of the one-dimensional nature of these materials. Thus, the Coulomb potential increases and the exciton binding energy gets stronger. In the case of CNTs, this energy can be several hundred meV and depends on the radius, chirality, and surrounding materials [68–75]. In experimental measurements, similar to theoretical results, it has been shown that excitonic effects are dominant in the optical response of CNTs [76]. Also, one-dimensional carbon chains such as polyenes or conjugated polymers show strong excitonic effects with binding energies varying between 200-900 meV [77–80]. Theoretical implementation of excitons in these studies following the Bethe-Salpeter equation (BSE) [81] has resulted in the prediction of exciton states and optical responses in semiconductors with high accuracies comparable to experimental findings. Since excitonic effects in CNTs and carbon chains considerably change their optical response spectra, it is expected that new hybrid CNT-carbyne systems in Fig. 1.2 to have distinct excitonic effects in their optical response, which are absent in isolated CNT and carbyne systems.

External static electric fields in materials can also modify their optical response. Modifications of the optical properties of materials with electrostatic field introduce a new study field so-called electro-optics, which have diverse applications in optical-based devices such as photodetectors [82], optical modulators [83] and materials characterization tools [84]. Electrostatic fields should be strong enough to observe noticeable changes in the electronic structure and optical response of systems. Thus, the effect of strong DC field should be treated non-perturbatively in the system. Since Franz [85] and Keldysh [86] studied modifications of the optical response of bulk semiconductors with the presence of electrostatic fields, separately, the effect of DC electric fields in semiconductors are also referred to as the Franz-Keldysh (FK) effect. In the case of small quantum structures that resemble quantum wells, electrostatic fields result in the quantum-confined Stark effect [87]. Due to modifications in the potential of semiconductors under the DC field, electrons and holes can tunnel into the forbidden energy gap region and an exponential tail in the linear optical response below the band gap of semiconductors is seen [85, 86]. Another fingerprint of the FK effect in the optical response of semiconductors is the appearance of oscillatory peaks in the response above the band gap. The reason for this can be explained by the Airy function behavior of the optical response in this energy region [88]. Moreover, DC fields can break the inversion symmetry for centrosymmetric semiconductors and result in considerable even-order of nonlinear optical responses, which these orders are dipole-forbidden in the absence of DC fields. For the second-order nonlinear response, electric field-induced second harmonic (EFISH) is very important in the investigation of nonlinear optical response in centrosymmetric semiconductors [89–91].

In one-dimensional semiconductors, experimental measurements for GaN and CdS nanowires have shown that DC fields cause an exponential tail and oscillatory peaks in their optical response [92, 93]. Significant FK fingerprints in the experimental electro-absorption spectra in conjugated polymer chains such as polydiacetylene [94–96], one-dimensional metallic dioxime complexes [97] and CNTs [98] show that these materials optical properties are significantly affected by external DC fields. Also, modulations of the optical response in the presence of DC fields have been calculated theoretically for various semiconducting quantum wires [88, 99–104].

The effect of external electrostatic fields in semiconducting CNTs and GNRs depends on the direction of applied DC fields. Fields along the infinite periodic direction (longitudinal direction) and finite direction (transverse direction) of these systems have different effects in their optical response. Transverse DC fields effects on the optical response of single- and multi-layered GNRs and boron nitride nanoribbons (BNNRs) have been extensively studied. Modulations of the band structure and transformation from metallic to semiconducting behavior (band gap opening) or vice versa (band gap closing) have been reported in selected AGNRs and ZGNRs in single- and multi-layered forms, as well as in BNNRs [105–114]. Furthermore, strong electro-absorption resonances in the optical response of GNRs due to the broken inversion symmetry under transversal DC fields have been achieved [107]. Despite a decent amount of research in transversal fields effects, studies for longitudinal fields in GNRs are rare. Applying periodic DC fields in the longitudinal direction of AGNRs and ZGNRs results in modifications of their electronic structure and optical response, which depend on the period and strength of the field [115]. These periodic fields do not show FK fingerprints in these structures, due to the small number of chosen unit cells that DC fields are extended over them in that study. In CNTs with various chiralities, the effect of longitudinal electrostatic fields, which are extended over a sufficient number of unit cells, show considerable FK oscillation peaks above the band gap [116]. It can computationally be very demanding to include a sufficient number of unit cells in these methods to approach the uniform field, especially when there is a large number of atoms in the unit cell of the system.

There are few studies considering the nonlinear optical response of semiconductors in the presence of strong DC fields. In Ref. [117], the author has provided a general N-photon absorption process in semiconductors under effects of electrostatic fields, in which in the case of the second-order nonlinear response, FK-like effects, i.e., oscillation peaks above and tunneling-assisted photon absorptions below every one- and two-photon resonances are expected. In quantum wires, two-photon absorptions under DC fields show FK-like effects in this process [118], which is in agreement with results of Ref. [117]. Moreover, in polyene chains, an agreement between experimental and theoretical EFISH has been reported [119].

1.1 This thesis

The focus of this thesis is the calculation of the optical response of one-dimensional semiconductors considering the following cases: (i) applying electrostatic fields on the optical response, and (ii) beyond the independent-electron picture and calculating the optical response including electron-hole interactions. To this end, three calculation steps will be followed. Firstly, the electronic structure of the introduced semiconductors will be calculated. Secondly, the single-electron optical response under the influence of external optical fields will be obtained. Finally, the electronic structure and optical response of systems under the effects of DC fields or excitons will be calculated.

The method for obtaining the electronic structure of systems in this thesis is the TB model. The reason is that this method is capable of obtaining the electronic structure with a denser k-points choice, which is necessary for smooth optical response spectra. For calculating the optical response in the low energy limit around the band gap in one-dimensional carbon-based semiconductors in this thesis, a simple model is to take one π-orbital for each carbon atom and use the 1NN approximation. For carbon chains in paper **??**, TB parameters are based on approximated values for carbon-carbon and carbon-nitrogen bonds. For GNRs in paper **??**, TB hopping parameters for carbon-carbon π-bonds are extracted from fitting TB band structure against a pseudopotential method [120]. For hybrid CNT-carbyne systems in paper **??**, a DFT calculation is performed using the ABINIT package to extract TB parameters by fitting a TB band structure against that of the DFT method.

For calculating the independent-electron linear and nonlinear optical response of systems, a quantum mechanical method using the time-dependent perturbation theory is employed. The effect of external optical fields can be calculated by adding harmonic-perturbation Hamiltonian term to the unperturbed Hamiltonian of the system. This method is comprehensively explained in various textbooks [121]. The method and obtained linear and nonlinear optical response equations in papers **??**, **??** and **??** will be briefly reviewed in the next chapter.

The independent-electron optical response enables the study of the modifications in the response with the presence of excitonic effects. The BSE is a highly capable method for calculating excitonic states and exciton binding energies in semiconductors [122]. This approach is used to calculate exciton binding energies and subsequently excitonic optical response of CNT-carbyne systems in paper **??**. Although theoretical excitonic effects in various CNTs [69, 70, 123–128] and carbon-based one-dimensional polymer chains [78–80] have been studied extensively, new hybrid CNT-carbyne systems are expected to have unique excitonic optical response that differs considerably from isolated CNT and carbyne systems. Four exciton configurations can be found in the hybrid system, i.e., electrons and holes are on one subsystem, electrons are on CNT and holes are on carbyne and vice versa. Alongside the BSE for calculating excitonic effects, the Wannier approximation is also used to compute exciton binding energies and excitonic optical response of CNT-carbyne systems, and results are compared with BSE results. The Wannier approach is a simplified version of the BSE method with approximations. Although this method does not have the complexity of BSE and is computationally faster, it is not as accurate as BSE and restricted to a two-band model of a semiconductor, which makes it difficult to obtain the full optical response of systems with more than two bands in their electronic structure.

Strong external electrostatic fields also modify the electronic structure and optical response of semiconductors. These modifications for one-dimensional semiconductors are studied in papers **??** and **??**. A novel formalism for calculating DC field effects on two-band one-dimensional semiconductors along the periodic axis of the system and using the density matrix formalism and Green's function method is provided in paper **??**. Then, the FK effect on the linear and nonlinear optical response for polyacetylene chains are calculated. It is shown that the dipole formalism of finite structures converges to the momentum method for infinite systems. Therefore, the size effect in the linear and nonlinear optical response of these systems with and without DC fields effects are studied. In paper **??**, the model is extended to a general multiband one-dimensional semiconductor, then DC fields are applied in both transversal and longitudinal directions of AGNRs. Transversal fields, which are along the finite direction of AGNRs, lead to modifications in the band structure and optical response. Longitudinal fields, which are along the infinite direction of these systems, cause non-perturbative FK effects. Moreover, fields can break the inversion symmetry and result in EFISH in AGNRs. In addition, similar to polyacetylene chains, finite AGNRs optical response with increasing length is studied. Furthermore, the effect of increasing the width of AGNRs are considered to study the convergence of the optical response of AGNRs to the two-dimensional graphene.

Graphene has remarkable potential in electro-optical applications [129, 130].

It has been shown that electrostatic fields break the band structure of two-dimensional graphene to a set of energy states referred to as "Wannier-Stark" (WS) ladder, and optical transitions occur between these states [131]. Because wide AGNRs show a similar behavior of graphene sheets, in paper **??**, the method for calculating DC fields effects in one-dimensional semiconductors is extended to two-dimensional semiconductors to obtain graphene optical response and compare it with wide AGNRs.

The thesis is organized as follows: subsequently in Chap. 2, theories and methods used for calculations in this thesis are explained. Chap. 3 summarizes the results of calculations in papers. Next, conclusions are provided in Chap. 4. All papers, which this thesis is based on, are collected at the end of the thesis.

Chapter 2

Theory and Methods

This chapter provides theories and computational methods used to obtain results in this thesis. Most of theories are available in the papers at the end of the thesis, and complementary descriptions and equations will be presented in this chapter.

The optical response of systems is based on defining the electronic structure, where the tight-binding (TB) method is used for this reason. Here, TB formalism alongside a brief introduction of the density functional theory (DFT) model, which is used for TB fitting in paper **??** will be presented. Then, theoretical methods for obtaining the independent-electron optical response, as well as excitonic and electrostatic fields effects on the electronic structure and optical response will be introduced.

2.1 Electronic structure

In the atomic scale, the electronic structure has a central role in defining the characteristics, as well as optical and electrical properties of materials. The electronic structure in this thesis is obtained using DFT and TB, which are two capable theoretical methods for this reason.

2.1.1 Density functional theory

Theoretical calculations of the electronic structure for many-electron systems such as crystals and bulk materials were successfully implemented using the DFT method after the advent of modern computers and utilizing their computational power in the middle of the 20^{th} century. DFT is based on two theorems [30]: first, the ground state of a system uniquely depends on the electron density of that system, which extensively reduces the complexity of many interacting-particle systems, and second, the correct ground state is a unique functional of the electron density, which minimizes the total energy of the system. This model was further improved by replacing particle-particle interactions using "exchange-correlation" terms [132], despite the exact functional form of exchange-correlation terms is unknown. Hence, these functionals can be approximated by the density at any evaluated point, which is called as local density approximation (LDA).

In this thesis, DFT is used to calculate the electronic structure of hybrid CNT-carbyne systems by the ABINIT software package [133]. As mentioned earlier, DFT underestimates the band gap energy for semiconductors. Therefore, a GW correction on top of DFT can compensate the band gap energy problem. The GW method is computationally very demanding and complex, hence in this thesis, a scissors shift based on previous GW calculations is applied to obtain a more accurate band gap for the system.

2.1.2 Tight-binding method

Compared to DFT, TB is a simpler quantum mechanical method to obtain the electronic structure of semicondutors with much less computational costs. The electronic structure for both bulk semiconductors and finite molecules can be calculated using the TB formalism. In this method, the potential energy of atomic sites is considered to be sufficiently strong, in which electrons are localized on those sites. Thus, Hamiltonian of the system can be approximated by atomic Hamiltonian on each atomic site with atomic Schrödinger equation $H_{at}\psi_n(\boldsymbol{r}) = E_n\psi_n(\boldsymbol{r})$, where ψ_n and E_n is the atomic wave function and energy, respectively. If a finite structure without electron-electron interactions is considered, the total wave function of the system $\psi(\boldsymbol{r})$ in the TB model can be approximated by a linear combination of atomic orbitals (LCAO) via $\psi(\boldsymbol{r}) = \sum_{n,i} a_n\phi_i(\boldsymbol{r} - \boldsymbol{R}_n)$, with i is the type of orbital ϕ, a is the expansion coefficient and $\boldsymbol{R}_n$ is the position of atom n in the structure. From Schrödinger equation for the system, Hamiltonian H and overlap S matrix elements in the Dirac notation are

$$\begin{aligned} H_{in,jm} &= \big\langle \phi_i(\boldsymbol{r} - \boldsymbol{R}_n)\big|H(\boldsymbol{r})\big|\phi_j(\boldsymbol{r} - \boldsymbol{R}_m)\big\rangle, \\ S_{in,jm} &= \big\langle \phi_i(\boldsymbol{r} - \boldsymbol{R}_n)\big|\phi_j(\boldsymbol{r} - \boldsymbol{R}_m)\big\rangle. \end{aligned} \tag{2.1}$$

Choosing the orbital basis depends on the atomic structure and target energy interval in the calculation. For carbon-based structures, the sp^3 basis can describe the electronic structure for a broad energy region. For the considered energy region and the atomic structure of materials in this thesis, the orthogonal atomic basis is utilized, i.e., overlap matrix elements are taken as Kronecker delta δ_{ij}. Moreover, instead of the sp^3 orbital basis, one π-orbital per atom is considered. This choice has a benefit of reducing unnecessary computational costs. Choosing a proper orbital basis and using Eq. (2.1), Hamiltonian and overlap matrices are constructed to solve the eigenvalue problem

$$\left(\overleftrightarrow{H} - E\overleftrightarrow{S}\right) \cdot \vec{a} = 0, \tag{2.2}$$

where E is the energy of the system.

Infinite systems are infinite repeating atomic units that are called unit cells. If N is the number of unit cells and ϕ_i is an atomic orbital with i as the orbital type, then the electron wave function in the structure can be expanded in terms of Bloch functions of that orbital

$$\Phi_{i\boldsymbol{k}}(\boldsymbol{r}) = \frac{1}{\sqrt{N}} \sum_{\boldsymbol{R}} e^{i\boldsymbol{k}\cdot\boldsymbol{R}} \phi_i(\boldsymbol{r} - \boldsymbol{R}), \tag{2.3}$$

where $\boldsymbol{R}$ is the position of each unit cell, which summed over all unit cells and $\boldsymbol{k}$ is the wavevector. This function satisfies the Bloch's theorem $\Phi_{\boldsymbol{k}}(\boldsymbol{r} + \boldsymbol{R'}) = e^{(i\boldsymbol{k}\cdot\boldsymbol{R'})}\Phi_{\boldsymbol{k}}(\boldsymbol{r})$. Thus, crystal wave function $\Psi_{\boldsymbol{k}}(\boldsymbol{r})$ is a linear combination of Bloch functions, considering all atomic orbitals

$$\Psi_{\boldsymbol{k}}(\boldsymbol{r}) = \sum_i a_i \Phi_{i\boldsymbol{k}}(\boldsymbol{r}). \tag{2.4}$$

After defining atomic orbitals, Hamiltonian and overlap matrix elements are constructed as follows

$$\begin{aligned} H_{ij} &= \frac{1}{N} \sum_{\boldsymbol{RR'}} e^{i\boldsymbol{k}\cdot(\boldsymbol{R}-\boldsymbol{R'})} \big\langle \phi_i(\boldsymbol{r} - \boldsymbol{R'}) \big| H(\boldsymbol{r}) \big| \phi_j(\boldsymbol{r} - \boldsymbol{R}) \big\rangle = \sum_{\boldsymbol{R}} e^{i\boldsymbol{k}\cdot\boldsymbol{R}} t_{ij}(\boldsymbol{R}), \\ S_{ij} &= \frac{1}{N} \sum_{\boldsymbol{RR'}} e^{i\boldsymbol{k}\cdot(\boldsymbol{R}-\boldsymbol{R'})} \big\langle \phi_i(\boldsymbol{r} - \boldsymbol{R'}) \big| \phi_j(\boldsymbol{r} - \boldsymbol{R}) \big\rangle = \sum_{\boldsymbol{R}} e^{i\boldsymbol{k}\cdot\boldsymbol{R}} s_{ij}(\boldsymbol{R}). \end{aligned} \tag{2.5}$$

Because there are terms $\boldsymbol{R} - \boldsymbol{R'}$ in these equations, one $\boldsymbol{R}$-summation is performed to simplify the equations, which results in the appearance of a factor N. TB parameters $t_{ij}(\boldsymbol{R})$ and $s_{ij}(\boldsymbol{R})$ are hopping and overlap matrix elements between atomic orbitals located in neighboring sites, respectively, which can be obtained by either experiments or fitting against *ab initio* calculations like DFT. To obtain the band structure of crystals, the orbital basis and number of interacting neighbors that atomic orbitals extend over them must be defined. Then, an eigenvalue problem similar to Eq. (2.2) is constructed, in which eigenvalues of this equation result in the band structure of any periodic system.

2.2 Single-electron optical response

External electromagnetic fields induce polarization in semiconducting materials. Electric polarization $P(t)$ is the response of the system to the electric field part F_t (optical field) by a response function χ, which is referred to as the electrical susceptibility. Therefore, in the linear regime at any time t, polarization is the integration of the response knowledge of all times t' prior to t via

$$P(t) = \varepsilon_0 \int_{-\infty}^{t} \chi(t - t')F_t(t')\, dt', \tag{2.6}$$

where ε_0 is the vacuum permittivity. Here, vector parameters are written as scalers to simplify the notation for obtaining the optical response in one direction. Hence, response functions are scalers instead of tensors. Also, the electric dipole approximation is considered, in which the susceptibility is independent of the position in the system. Therefore, Eq. (2.6) which is in the time domain can be convoluted to the frequency domain

$$P(\omega) = \varepsilon_0 \chi(\omega) F_\omega. \tag{2.7}$$

When the optical field is weak, the linear response can satisfactorily describe the response of the system. For stronger fields, the full response of the system is not in a simple linear form. Therefore, Eq. (2.6) is expanded as a power series of the optical field

$$\begin{aligned} P(t) = \varepsilon_0 \Bigg\{ &\int_{-\infty}^{t} \chi^{(1)}(t - t')F_t(t')\, dt' \\ &+ \int_{-\infty}^{t}\int_{-\infty}^{t} \chi^{(2)}(t - t'_1, t - t'_2)F_t(t'_1)F_t(t'_2)\, dt'_1 dt'_2 \\ &+ \int_{-\infty}^{t}\int_{-\infty}^{t}\int_{-\infty}^{t} \chi^{(3)}(t - t'_1, t - t'_2, t - t'_3)F_t(t'_1)F_t(t'_2)F_t(t'_3)\, dt'_1 dt'_2 dt'_3 + \cdots \Bigg\}, \end{aligned} \tag{2.8}$$

where $\chi^{(1)}$ is the linear, $\chi^{(2)}$ and $\chi^{(3)}$ are the second and third order nonlinear optical susceptibility, respectively. Similar to Eq. (2.7), the Fourier transformation can convert Eq. (2.8) to the frequency domain

$$\begin{gathered} P(\omega) = P^{(1)}(\omega) + P^{(2)}(\omega) + P^{(3)}(\omega) + \cdots, \\ P^{(1)}(\omega) = \varepsilon_0 \chi^{(1)}(\omega) F_\omega, \\ P^{(2)}(\omega) = \varepsilon_0 \chi^{(2)}(\omega = \omega_1 + \omega_2) F_{\omega_1} F_{\omega_2}, \\ P^{(3)}(\omega) = \varepsilon_0 \chi^{(3)}(\omega = \omega_1 + \omega_2 + \omega_3) F_{\omega_1} F_{\omega_2} F_{\omega_3}. \end{gathered} \tag{2.9}$$

In the following, the response function will be obtained using the time-dependent quantum perturbation theory for both finite and infinite one-dimensional semiconductors.

2.2.1 Finite system

The response function in this thesis is obtained by a semi-quantum mechanical approach, in which one-dimensional materials are considered as quantum systems with the x-axis as their long direction and optical fields as classical fields along this axis. The optical field Hamiltonian $\hat{H}_1 = e\hat{x}F_t$, which e is the electron charge and $\hat{x}$ is the position operator along the x-axis, perturbs the stationary Hamiltonian $\hat{H}_0$ of the system. Thus, the total Hamiltonian is

$$\hat{H} = \hat{H}_0 + \hat{H}_1. \tag{2.10}$$

The optical field Hamiltonian can be treated harmonically $\hat{H}_1 = 1/2\{\hat{h}_1 e^{-i\omega t} + h.c.\}$ with ω as the frequency of the optical field and $h.c.$ is the hermitian conjugate. Using Hamiltonian (2.10), the time-dependent Schrödinger equation is constructed, considering $\psi \equiv \psi(x,t)$ as the wave function, which defines the state of the system

$$i\hbar \frac{\partial \psi}{\partial t} = \hat{H}\psi. \tag{2.11}$$

This equation can not be solved because of the unknown wave function ψ. To solve the problem, the wave function is written in a complete set of known energy states of the system

$$\psi = \sum_n a_n(t)\varphi_n e^{-i\omega_n t}, \tag{2.12}$$

where $a_n(t)$ is time-dependent expansion coefficients and φ_n is stationary states of the system with the eigenvalue equation $\hat{H}_0\varphi_n = E_n\varphi_n$ and energy eigenstates of $E_n = \hbar\omega_n$. Thus, the exact equation form of $a_n(t)$ yields defining the state ψ of the system. To this end, Eq. (2.12) is replaced into Eq. (2.11) and the orthogonal condition between energy states $\langle\varphi_n|\varphi_m\rangle = \delta_{nm}$ is considered

$$\frac{\partial a_m(t)}{\partial t} = \frac{1}{2i\hbar}\sum_n a_n(t)\Big\{\langle\varphi_m|\hat{h}_1|\varphi_n\rangle e^{-i\omega t} + c.c.\Big\}e^{i\omega_{mn}t},\ \omega_{mn} = \omega_m - \omega_n. \tag{2.13}$$

To find $a_n(t)$ from Eq. (2.13), the power series of perturbation $a_n(t) = a_n^{(0)}(t) + a_n^{(1)}(t) + a_n^{(2)}(t) + \cdots$ is introduced. Since $\langle\varphi_m|\hat{h}_1|\varphi_n\rangle$ has one power of the perturbation, Eq. (2.13) results in the following equation for an arbitrary order p

$$a_m^{(p)} = \frac{1}{2i\hbar}\sum_n \int dt\, a_n^{(p-1)}\Big\{\langle\varphi_m|\hat{h}_1|\varphi_n\rangle e^{-i\omega t} + c.c.\Big\}e^{i\omega_{mn}t}. \tag{2.14}$$

From Eq. (2.14), it can be concluded that $\partial a_n^{(0)}(t)/\partial t = 0$, i.e., the zeroth order of the expansion coefficient is a constant value in time. Also, the zeroth order can be interpreted as the lack of perturbation in the system. The orthogonality of φ_ns and normalization of the wave function $\langle\psi|\psi\rangle = 1$ result in $\sum_n |a_n^{(0)}|^2 =$

1. $|a_n^{(0)}|^2$ can be interpreted as the probability of the unperturbed system to be in state φ_n. Thus in the thermal equilibrium, $f(E_n) = |a_n^{(0)}|^2$, with $f(E_n)$ is the energy-dependent probability distribution function. The first and second orders of expansion coefficients can be derived from Eq. (2.14) after performing the time integration

$$a_m^{(1)} = -\frac{1}{2}\sum_n a_n^{(0)} \left\{ \frac{\langle \varphi_m|\hat{h}_1|\varphi_n\rangle e^{-i\omega t}}{E_{mn} - \hbar\omega} + \frac{\langle \varphi_m|\hat{h}_1^\dagger|\varphi_n\rangle e^{i\omega t}}{E_{mn} + \hbar\omega} \right\} e^{i\omega_{mn} t}, \tag{2.15}$$

$$\begin{aligned} a_m^{(2)} = \frac{1}{4}\sum_{n,l} a_n^{(0)} \Bigg\{ & \frac{\langle \varphi_m|\hat{h}_1|\varphi_l\rangle\langle \varphi_l|\hat{h}_1|\varphi_n\rangle e^{-2i\omega t}}{(E_{mn} - 2\hbar\omega)(E_{ln} - \hbar\omega)} + \frac{\langle \varphi_m|\hat{h}_1^\dagger|\varphi_l\rangle\langle \varphi_l|\hat{h}_1|\varphi_n\rangle}{(E_{ln} - \hbar\omega)E_{mn}} \\ & + \frac{\langle \varphi_m|\hat{h}_1^\dagger|\varphi_l\rangle\langle \varphi_l|\hat{h}_1^\dagger|\varphi_n\rangle e^{2i\omega t}}{(E_{mn} + 2\hbar\omega)(E_{ln} + \hbar\omega)} + \frac{\langle \varphi_m|\hat{h}_1|\varphi_l\rangle\langle \varphi_l|\hat{h}_1^\dagger|\varphi_n\rangle}{(E_{ln} + \hbar\omega)E_{mn}} \Bigg\} e^{i\omega_{mn} t}. \end{aligned} \tag{2.16}$$

Since the system tends to decay back to the ground state, in these equations, a damping term $i\hbar\Gamma$ is added to the optical field energy $\hbar\omega$ to compensate the ignored system losses. Obtaining higher orders of expansion coefficients a_n from Eq. (2.14) are skipped to explicitly be derived because the first and second-order nonlinear optical response is only considered in this thesis for calculations.

Knowing different orders of expansion coefficients a_n, a time-dependent physical observable $X(t)$ can be calculated by evaluating the expectation value of the response observable $X(t) = \langle\psi|\hat{X}|\psi\rangle$

$$\begin{aligned} X(t) = \sum_{m,n} \langle \varphi_n|\hat{X}|\varphi_m\rangle (& a_n^{(0)*}a_m^{(0)} + a_n^{(0)*}a_m^{(1)} + a_n^{(1)*}a_m^{(0)} \\ & + a_n^{(2)*}a_m^{(0)} + a_n^{(0)*}a_m^{(2)} + a_n^{(1)*}a_m^{(1)} + \cdots) e^{-i\omega_{mn} t}. \end{aligned} \tag{2.17}$$

The first term inside the parentheses is $a_n^{(0)*}a_m^{(0)} = f(E_n)\delta_{nm}$, which shows the state of the system without the optical field perturbation. The second and third terms correspond to the linear part of the observable $X(t)$. The next three terms reflect the second-order nonlinear part of $X(t)$. Higher orders are skipped to explicitly be written in Eq. (2.17) because of deriving optical response equations up to the second order in this thesis.

Before deriving final expressions for the linear and nonlinear optical response, Fourier decomposition is used to convert the time-dependent response into frequency components up to the second order

$$X(t) \approx \frac{1}{2}\Big\{ X^{(0)} + X^{(1)}(\omega)e^{-i\omega t} + \frac{1}{2}X^{(2)}(\omega)e^{-2i\omega t} + c.c. \Big\}, \tag{2.18}$$

where the first term is the static contribution, in which there is no perturbation in the system. The second term and its corresponding complex conjugate term give the linear contribution. The last term and its corresponding complex conjugate results in the second-order nonlinear response. Therefore, from Eqs. (2.15)-(2.18)

$$X^{(1)}(\omega) = -\sum_{m,n} f_{nm} \frac{\left\langle \varphi_m \middle| \hat{h}_1 \middle| \varphi_n \right\rangle \left\langle \varphi_n \middle| \hat{X} \middle| \varphi_m \right\rangle}{E_{mn} - \hbar\omega}, \tag{2.19}$$

$$X^{(2)}(\omega) = \sum_{m,n,l} \frac{\left\langle \varphi_n \middle| \hat{X}_1 \middle| \varphi_m \right\rangle \left\langle \varphi_m \middle| \hat{h}_1 \middle| \varphi_l \right\rangle \left\langle \varphi_l \middle| \hat{h}_1 \middle| \varphi_n \right\rangle}{E_{mn} - 2\hbar\omega} \left\{ \frac{f_{ml}}{E_{ml} - \hbar\omega} + \frac{f_{nl}}{E_{ln} - \hbar\omega} \right\}, \tag{2.20}$$

where $f_{nm} = f(E_n) - f(E_m)$ is the population difference between states n and m. Defining the perturbation Hamiltonian and response function leads to obtaining the exact form of the response of the system. The frequency-dependent optical field perturbation Hamiltonian $\hat{h}_1 = e\hat{x}F_\omega$ causes polarization P in the system. Polarization is the total dipole moment of the system per unit volume, so the response operator is the dipole moment operator $\hat{X} = -e\hat{x}/L$, which L is the length of the one-dimensional system. Applying these into Eqs. (2.19) and (2.20) and using the relation between the induced polarization and optical field from Eq. (2.9) result in the linear and nonlinear optical susceptibility function $\chi(\omega)$, respectively. After some manipulations

$$\chi^{(1)}(\omega) = \frac{2e^2}{\varepsilon_0 L} \sum_{m,n} f(E_n) |x_{nm}|^2 \frac{E_{mn}}{E_{mn}^2 - (\hbar\omega)^2}, \tag{2.21}$$

$$\chi^{(2)}(\omega) = \frac{e^3}{\varepsilon_0 L} \sum_{m,n,l} \frac{x_{lm} x_{mn} x_{nl}}{E_{ml} - 2\hbar\omega} \left\{ \frac{f_{ln}}{E_{nl} - \hbar\omega} + \frac{f_{mn}}{E_{mn} - \hbar\omega} \right\}, \tag{2.22}$$

where $x_{nm} = \langle \varphi_n | \hat{x} | \varphi_m \rangle$ is dipole moment matrix elements. These equations can be numerically calculated by obtaining energy levels E_n and vectors φ_n by solving the eigenvalue problem in Eq. (2.2). Instead of the polarization, the current density $J(\omega)$ can be chosen as the response of the system to the external field. Choosing this response and using the equation $J(\omega) = \sigma(\omega)F_\omega$ result in the linear optical conductivity $\sigma(\omega)$. Current density is simply the time derivative of the polarization $J(t) = \partial P(t)/\partial t$, which in the frequency domain $J(\omega) = -i\omega P(\omega)$. Thus, the susceptibility can be converted to the conductivity via $\sigma(\omega) = -i\omega\varepsilon_0\chi(\omega)$.

2.2.2 Infinite system

For infinite systems, states of the system are in the form of φ_{nk} with $H_0\varphi_{nk} = E_{nk}\varphi_{nk}$. Here, E_{nk} is the unperturbed energy of the system for the quantum wavenumber k in the quantum band number n. The electron wave function in a periodic system is in the form of the Bloch function, which consists of a plane wave multiplied by a periodic function. These are explained comprehensively in textbooks [134]. Thus, Eqs. (2.21) and (2.22) are modified for the infinite response equations by including band indices

$$\chi^{(1)}(\omega) = \frac{2e^2}{\varepsilon_0 L} \sum_{m,n,k,k'} f(E_{nk}) |x_{nk,mk'}|^2 \frac{E_{mk',nk}}{E^2_{mk',nk} - (\hbar\omega)^2}. \tag{2.23}$$

Solving Eq. (2.2) for an infinite system results in the energy band structure E_{nk} and states φ_{nk}. The remaining problem in solving Eq. (2.23) is that the operator $\hat{x}$ is ill-defined for infinite structures. Therefore, dipole moment matrix elements cannot be evaluated. To solve this issue, well-defined momentum matrix elements $p_{nk,mk'}$ are used from the equation $x_{nk,mk'} = \hbar p_{nk,mk'}/imE_{nk,mk'}$, where $x_{nk,mk'} = \langle\varphi_{nk}|\hat{x}|\varphi_{mk'}\rangle$, $p_{nk,mk'} = \langle\varphi_{nk}|\hat{p}|\varphi_{mk'}\rangle$ and $E_{nk,mk'} = E_{nk} - E_{mk'}$. This equation is obtained from the commutator relation between the unperturbed Hamiltonian H_0 and the position operator via $\langle\varphi_{nk}|[H_0, \hat{x}]|\varphi_{mk'}\rangle$ and only valid for interband contributions ($n \neq m$). Using the momentum instead of the dipole moment and considering only interband transitions

$$\chi_1^{\text{inter}}(\omega) = \frac{2e^2\hbar^2}{\varepsilon_0 m^2 L} \sum_{\substack{m,n,k \\ m\neq n}} f(E_{nk}) \frac{|p_{nmk}|^2}{E_{mnk}(E^2_{mnk} - (\hbar\omega)^2)}, \tag{2.24}$$

where $p_{nmk} = \langle\varphi_{nk}|\hat{p}|\varphi_{mk}\rangle$ and $E_{mnk} = E_{mk} - E_{nk}$. Similar modifications can be applied for the nonlinear response in Eq. (2.22) to obtain the second-order nonlinear optical susceptibility for infinite systems. If pure interband contributions are considered, the following equation is obtained from Eq. (2.22)

$$\chi_2^{\text{inter}}(\omega) = -\frac{2ie^3\hbar^3}{m^3\varepsilon_0 L} \sum_{\substack{m,n,l,k \\ m\neq n, m\neq l, n\neq l}} \frac{p_{lmk}p_{mnk}p_{nlk}}{E_{lmk}E_{mnk}E_{nlk}(E_{mlk} - 2\hbar\omega)} \times \left\{ \frac{f_{lnk}}{E_{nlk} - \hbar\omega} + \frac{f_{mnk}}{E_{mnk} - \hbar\omega} \right\}. \tag{2.25}$$

If intraband contributions ($n = m$) are considered, it is not allowed to use equation $x_{nk,mk'} = \hbar p_{nk,mk'}/imE_{nk,mk'}$. Therefore, another method is introduced by dividing the position operator $\hat{x}$ into two interband $\hat{x}^e$ and intraband $\hat{x}^i$ parts. Following the procedure in Ref. [135], the second-order nonlinear susceptibility for mixed inter- and intraband contributions is

$$\chi_2^{\text{mixed}}(\omega) = \frac{3ie^3}{m^2\varepsilon_0 L} \sum_{\substack{m,n,k \\ m\neq n}} f(E_{nk}) \frac{p_{nmk}(p_{mnk})_{;k}}{(E^2_{mnk} - (2\hbar\omega)^2)(E^2_{mnk} - (\hbar\omega)^2)}, \tag{2.26}$$

where $(p_{mnk})_{;k}$ is the generalized derivative of momentum matrix elements with respect to k, which is $(p_{mnk})_{;k} = \partial p_{mnk}/\partial k - ip_{mnk}(\Omega_{mmk} - \Omega_{nnk})$ and $\Omega_{mnk} = i/V_{uc} \int u^*_{mk}(\boldsymbol{r})\partial u_{nk}(\boldsymbol{r})/\partial k d\boldsymbol{r}$ is the Berry connection between bands n and m. V_{uc} is the unit cell volume and $u_{nk}(\boldsymbol{r})$ is the periodic part of the Bloch wave function $\psi_{nk}(\boldsymbol{r}) = 1/\sqrt{N} u_{nk}(\boldsymbol{r}) exp(ikx)$.

2.3 Exciton states

Up until now, theoretical methods for obtaining the electronic structure and optical response of atomic systems in the independent-electron picture have been introduced. Both TB and DFT methods result in the electronic structure of semiconductors in unperturbed energy states or the ground state. Then, these results are used to obtain the linear and nonlinear optical response of the system. In the presence of optical fields, electrons can be excited into excited states of the system. Therefore, relying on the ground state electronic structure sometimes fails miserably describing such excitations in semiconductors. To better describe the optical response in the system, especially for lower-dimensional semiconductors, it is necessary to obtain the electronic structure beyond the independent-electron model. To this end, many-body excited states or excitons are considered in these materials.

2.3.1 Bethe-Salpeter equation

The ground state of a N_0-particle system can be constructed by the Slater determinant $|0\rangle = \big| |v_1\rangle, |v_2\rangle, \cdots, |v_N\rangle \big|$, where $|v_i\rangle$ is an occupied single-electron valence state. To simplify the notation, up and down spins are skipped to be written. A single excitation means that a single valence state $|v_i\rangle$ excites into a single excited state $|c_j\rangle$, which is shown by the state $|v_i \rightarrow c_j\rangle$. Considering spin, in fact, results in a singlet state $|v_i \rightarrow c_j\rangle \equiv |v_i c_j\rangle = \{|v_i \uparrow \rightarrow c_j \uparrow\rangle + |v_i \downarrow \rightarrow c_j \downarrow\rangle\}/\sqrt{2}$ with the total spin of zero. Many-body excited states can be constructed by a linear combination of these singlets

$$|exc\rangle = \sum_{i,j} A^{(exc)}_{v_i,c_j} |v_i c_j\rangle. \tag{2.27}$$

Now, the problem is setting up the Hamiltonian equation using this exciton basis to obtain unknown expansion coefficients $A^{(exc)}_{v_i,c_j}$ and corresponding energies E_{exc}. Following the procedure in Ref. [135] results in an equation known as the Bethe-Salpeter equation (BSE)

$$\big(E_{c_j} - E_{v_i}\big) A^{(exc)}_{v_i c_j} - \sum_{i',j'} \big\langle v_i c_j \big| V_C - 2V_x \big| v_{i'} c_{j'} \big\rangle A^{(exc)}_{v_{i'} c_{j'}} = E_{(exc)} A^{(exc)}_{v_i c_j}. \tag{2.28}$$

Here, E_v and E_c are quasiparticle valence and conduction energy levels, respectively, which can be obtained by DFT or TB. $\langle V_C \rangle$ and $\langle V_x \rangle$ are screened Coulomb and unscreened exchange terms.

Before explaining the obtained terms in the BSE (2.28), proper modifications in this equation must be applied to write it for infinite systems, which are periodic structures. For such systems with the periodicity in one direction as mentioned in Sec. 2.2.2, single-particle states have a band index (v or c) and wavenumber k as quantum numbers. Thus, excitonic states will be in the form of $|vck\rangle \equiv |vk \rightarrow ck\rangle$. In optical excitations, there might be phonon-assisted optical excitations, where the k-number for a valence band is different from that of a conduction band. Although these kinds of optical processes are essential for studying the optical response in indirect-band semiconductors, direct optical excitations are considered in our notation, where the ground and excited states have an identical k-number. Thus, Eq. (2.28) is rewritten as

$$\big(E_{ck} - E_{vk}\big) A^{(exc)}_{vck} - \sum_{v',c',k'} \big\langle vck \big| V_C - 2V_x \big| v'c'k' \big\rangle A^{(exc)}_{v'c'k'} = E_{(exc)} A^{(exc)}_{vck}. \quad (2.29)$$

Coulomb potential between electrons at position $\boldsymbol{r}$ and holes at position $\boldsymbol{r'}$ is $v(\boldsymbol{r} - \boldsymbol{r'}) = e^2/4\pi\varepsilon_0|\boldsymbol{r} - \boldsymbol{r'}|$. This potential is screened for Coulomb matrix elements by a dielectric function ε, which depends on the structure and surrounding materials. In contrast, exchange matrix elements are constructed via bare Coulomb potential [136]. Coulomb and exchange matrix elements can be obtained from following expressions

$$\big\langle vck \big| V_C \big| v'c'k' \big\rangle = \frac{1}{\varepsilon} \iint \psi^*_{ck}(\boldsymbol{r}) \psi_{c'k'}(\boldsymbol{r}) v(\boldsymbol{r} - \boldsymbol{r'}) \psi_{vk}(\boldsymbol{r'}) \psi^*_{v'k'}(\boldsymbol{r'}) d\boldsymbol{r} d\boldsymbol{r'}, \quad (2.30)$$

$$\big\langle vck \big| V_x \big| v'c'k' \big\rangle = \iint \psi^*_{ck}(\boldsymbol{r}) \psi_{c'k'}(\boldsymbol{r'}) v(\boldsymbol{r} - \boldsymbol{r'}) \psi_{vk}(\boldsymbol{r}) \psi^*_{v'k'}(\boldsymbol{r'}) d\boldsymbol{r} d\boldsymbol{r'}. \quad (2.31)$$

Here, $\psi_{\alpha k}(\boldsymbol{r})$ ($\alpha = v$ or c) is Bloch sums similar to Eq. (2.4) for electrons in conduction bands and holes in valence bands. By constructing Coulomb and exchange matrix elements in Eqs. (2.30) and (2.31) and applying them into BSE (2.29), excitonic states $A^{(exc)}$ and energies $E_{(exc)}$ can be calculated.

2.3.2 Wannier approximation

Calculating exciton states using the BSE is complicated and computationally very demanding. A proper alternative to avoid this complexity is using the Wannier model, which is a simplified BSE by a set of approximations. The first approximation is that this method is limited to a two-band model of a semiconductor. Second, the exchange term is ignored in this model. Next, the effective mass dispersion is applied for both valence and conduction bands

$$E_{ck} \approx E_g + \frac{\hbar^2 k^2}{2m_e}, \quad E_{vk} \approx -\frac{\hbar^2 k^2}{2m_h}, \quad E_{ck} - E_{vk} \approx E_g + \frac{\hbar^2 k^2}{2\mu},$$

where m_e, m_h and μ are electron, hole and electron-hole effective mass, respectively, and E_g is the energy gap between valence and conduction bands. The final approximation is taking the following equation

$$I_{\alpha k,\alpha' k'} \equiv \frac{1}{V_{uc}} \int u^*_{\alpha' k'}(\boldsymbol{r}') u_{\alpha k}(\boldsymbol{r}) d\boldsymbol{r} \approx \delta_{\alpha\alpha'}.$$

Using these approximations and BSE (2.29) and Eq. (2.30), as well as performing an inverse Fourier transform to convert the k-space to the real space, result in the following equation in the Hartree units

$$\left\{ E_g - \frac{1}{2\mu}\nabla^2 - \frac{1}{\varepsilon} v(\boldsymbol{r}) \right\} \psi^{\mathrm{W}}_{exc}(\boldsymbol{r}) = E_{exc} \psi^{\mathrm{W}}_{exc}(\boldsymbol{r}). \tag{2.32}$$

This Schrödinger-like equation is called as the Wannier equation and can be solved by defining a basis function for $\psi^{\mathrm{W}}_{exc}(\boldsymbol{r})$ and attractive screened Coulomb potential between electrons and holes $1/\varepsilon v(\boldsymbol{r})$. It should be noted that this equation depends on the relative motion of electron-hole pair with the distance of $\boldsymbol{r}$ between them.

2.3.3 Excitonic optical response

Results of excitonic states calculated using either the BSE or Wannier model can be used to obtain the excitonic optical response. Although higher orders of the excitonic optical response can be evaluated, the response is restricted to the linear regime in this thesis. The starting point is obtaining many-body momentum matrix elements $P_{exc} = \langle 0|\hat{P}|exc\rangle$. $\hat{P}$ is the many-body momentum operator, which is the total momentum of single-electron momentum operators for a N_0-particle system $\hat{P} = \sum_n^{N_0} \hat{p}_n$. Solving exciton problem from the BSE (2.29) results in exciton eigenstates A^{exc}_{vck}. Thus, excitonic momentum matrix elements are simply

$$P_{exc} = \sum_{vck} A^{(exc)}_{vck} p_{vck}.$$

Now, the optical susceptibility function can be obtained using many-body momentum matrix elements and exciton energy states via

$$\chi^{(1)}(\omega) = \frac{2e^2\hbar^2}{\varepsilon_0 m^2 L} \sum_{exc} \frac{|P_{exc}|^2}{E_{exc}(E^2_{exc} - (\hbar\omega)^2)}. \tag{2.33}$$

In the Wannier approach, momentum matrix elements are different from those of the BSE. As a simplification, the dependency of the single-particle momentum matrix elements p_{mnk} to the wavenumber k is omitted, and these elements are considered as a fixed value p_0 for each valence and conduction band pair evaluated at a k-point corresponding to the minimum gap between these two bands. Then, many-body momentum matrix elements can be written as

$$P_{exc} = \langle 0|\hat{P}|exc\rangle = \sqrt{2}\sum_{k} \psi_k^{\mathrm{W}} p_0 = \sqrt{2L} p_0 \psi_{exc}^{\mathrm{W}}(0),$$

where, $\psi_{exc}^{\mathrm{W}}(0)$ is the Wannier exciton wave function evaluated at the origin. Hence, the linear optical susceptibility is

$$\chi^{(1)}(\omega) = \frac{4e^2\hbar^2|p_0|^2}{\varepsilon_0 m^2} \sum_{exc} \frac{|\psi_{exc}^{W}(0)|^2}{E_{exc}(E_{exc}^2 - (\hbar\omega)^2)}. \tag{2.34}$$

2.4 Static electric field and Franz-Keldysh effect

This section covers methods used in the calculation of the linear and nonlinear optical response of one-dimensional semiconductors under the effect of strong electrostatic fields. Many-body excitonic effects are excluded because the purpose of this section is only to show the effect of DC fields on the electronic structure and optical response of semiconductors. Different directions for electrostatic fields have different effects in quasi-one-dimensional semiconductors. Here, these fields are applied in two directions: (i) along with the long-axis of one-dimensional semiconductors, which is called the longitudinal direction, and (ii) perpendicular to the long axis, which is entitled as the transverse direction. Moreover, both finite and infinite semiconductors will be studied. Furthermore, methods will be extended to two-dimensional semiconductors to study the behavior of wide one-dimensional semiconductors compared to their two-dimensional counterparts.

2.4.1 Transversal DC fields

Transversal fields perturb the system by inducing dipole moments in the field direction and cause changes in the electronic structure and subsequently in the optical response of one-dimensional semiconductors. If the DC field is taken in y-direction in Fig. 1.3 as F_{DC}^{y}, then the DC field Hamiltonian is $\hat{H}_{\mathrm{DC}} = e\hat{y}F_{\mathrm{DC}}^{y}$. Thus, the system Hamiltonian before applying the optical field perturbation is

$$\hat{H} = \hat{H}_0 + \hat{H}_{\mathrm{DC}}.$$

This Hamiltonian is used to construct the eigenvalue equation. Evaluated eigenvalues and eigenvectors of this equation are used to construct transition energies and dipole moment matrix elements between energy states for finite systems, as well as transition energies and momentum matrix elements between bands for infinite systems. Then, these results are substituted into Eqs. (2.21) and (2.22) for finite systems and Eqs. (2.24)-(2.26) for infinite systems to obtain the linear and nonlinear optical susceptibility.

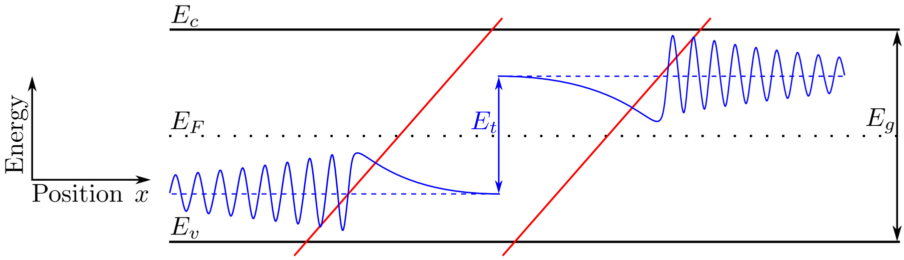

Fig. 2.1: The effect of DC fields in the x-direction on the energy structure of a semiconductor with the optical gap of E_g. E_c, E_v and E_F are conduction, valence and Fermi energy states, respectively. Tilted red states are the result of the DC field effect on the energy structure of the system. Electron and hole states are shown in blue waves. E_t is the transition energy resulted from the field-induced tunneling across the gap.

2.4.2 Longitudinal DC fields

For DC fields along the longitudinal direction, e.g., x-direction in Fig. 1.3, the field direction is along the periodic direction of the system. Thus, it is expected to obtain different results compared to the transversal field direction. If a finite system is considered, the procedure of calculating electrostatic fields effects on the electronic structure and optical response is similar to the transversal fields, in which the DC field Hamiltonian $\hat{H}_{\mathrm{DC}} = e\hat{x}F^{x}_{\mathrm{DC}}$ perturbs the system. If an infinite system is considered, one way to calculate the DC field effects is to include the periodic field, which extends over several unit cells of the system [115]. Taking a sufficient number of unit cells to calculate the Franz-Keldysh (FK) effect requires a heavy usage of computational resources. Thus, this method is not an efficient calculation method. In the following, a method will be introduced to avoid such a demanding computational method. Before continuing the calculation method, a brief description of DC fields effects on periodic systems is provided.

DC fields along the periodic direction tilt the potential of semiconductors and change the electronic structure as shown schematically in Fig. 2.1. As a result, the wave function of electrons and holes can penetrate to the forbidden gap region. Hence, optical transitions can occur with energy E_t, which is smaller than the gap energy E_g. Therefore, an exponential tail in the optical response below the band gap in semiconductors is seen [88]. Also, under the influence of longitudinal DC fields, the electron and hole wave function behaves like the Airy function. As a result of such behavior, the optical response of semiconductors shows oscillatory peaks above the band gap resonance [88].

DC fields lift the energy degeneracy in periodic structures and result in the localization of electron states in each lattice site. These localized states are referred to as the Wannier-Stark (WS) ladder and separated in space with the Hamiltonian $\hat{H}_{\mathrm{DC}}$ [137]. Also, field-induced couplings between bands are ignored because there are no degenerate bands in the studied systems in this thesis [138]. Taking this approximation into account enables writing equations for a single valence and conduction band pair (n, m). The remaining problem is solving the WS Hamiltonian equation $H_{\rm WS}\psi^{(p)}_{mnk} = E^{(p)}_{mn}\psi^{(p)}_{mnk}$. p is the index of WS states in valence and conduction bands with the corresponding wave function $\psi^{(p)}_{mnk}$ and energies $E^{(p)}_{mn}$. Considering this band pair, the Hamiltonian can be written as

$$H_{\rm WS} = E_{mnk} + ieF^{x}_{\rm DC}\Big\{\frac{d}{dk} + i(\Omega_{mmk} - \Omega_{nnk})\Big\}, \tag{2.35}$$

where E_{mnk} is the energy difference between valence and conduction band pair. The WS Hamiltonian equation can be used for setting up the eigenvalue problem and solving it by introducing the following WS wave function

$$\psi^{(p)}_{mnk} = \frac{1}{\sqrt{K}}\exp\Bigg\{-\frac{1}{eF^{x}_{\rm DC}}\Bigg(E^{(p)}_{mn}k - \int_0^k E_{mnk'}dk'\Bigg)\Bigg\}, \tag{2.36}$$

where K is the extent of the Brillouin zone along the DC field direction. Substituting this WS wave function into the WS Hamiltonian equation (2.35) and applying the Bloch boundary condition $\psi^{(p)}_{mnk} = \psi^{(p)}_{mn(k+K)}$, WS energy states are obtained

$$E^{(p)}_{mn} = \frac{2\pi peF^{x}_{\rm DC}}{K} + \frac{1}{K}\int_0^K \Big\{E_{mnk} + i(\Omega_{mmk} - \Omega_{nnk})\Big\}dk. \tag{2.37}$$

Under strong longitudinal DC fields, Eq. (2.37) shows that energy bands of a semiconductor are discretized into WS ladder.

For obtaining the DC optical response, a density matrix formalism is introduced using the Hamiltonian $\hat{H} = \hat{H}_0 + \hat{H}_1$, where $\hat{H}_1 = e(F_t + F^{x}_{\rm DC})\hat{x}$ is the total external perturbation caused by optical and DC fields. Here, DC fields effects in the system are treated non-perturbatively. The commutator between density matrix ρ and Hamiltonian H can be written by the Liouville equation $-i\hbar\partial\hat{\rho}/\partial t = [\hat{\rho}, \hat{H}]$. To solve this equation, the position operator $\hat{x}$ is divided into inter- $\hat{x}^e$ and intraband $\hat{x}^i$ parts. It can be shown that the inter- and intraband parts of the position operator in the crystal are [139]

$$x^{e}_{mnk} = \Omega_{mnk}, \quad [\hat{x}^i, \hat{\rho}]_{mnk} = i(\rho_{mnk})_{;k}.$$

Using the inter- and intraband parts of position operator and the Liouville equation, density matrix elements are

$$\begin{aligned} -i\hbar\frac{\partial\rho_{mnk}}{\partial t} + E_{mnk}\rho_{mnk} &= -ieF(\rho_{mnk})_{;k} \\ &+eF\sum_{l}\left\{\rho_{mlk}\Omega_{lnk}\bar{\delta}_{ln} - \Omega_{mlk}\rho_{lnk}\bar{\delta}_{ml}\right\}, \end{aligned} \tag{2.38}$$

where $F = F_t + F^x_{\rm DC}$ is the total electric field and $\bar{\delta}_{mn} = 1 - \delta_{mn}$ is 0 for $m = n$ and 1 for $m \neq n$. Because of the ignored field-induced couplings between energy bands [140], terms $F^x_{\rm DC}\Omega_{mnk}$ are ignored. Therefore, Eq. (2.38) can be rewritten as

$$\begin{aligned} -i\hbar\frac{\partial \rho_{mnk}}{\partial t} + H_{\rm WS}\rho_{mnk} &= -ieF_t(\rho_{mnk})_{;k} \\ +eF_t\sum_l \left\{\rho_{mlk}\Omega_{lnk}\bar{\delta}_{ln} - \Omega_{mlk}\rho_{lnk}\bar{\delta}_{ml}\right\}. \end{aligned} \tag{2.39}$$

Density matrix elements can be obtained by introducing the following Green's function equation

$$-i\hbar\frac{\partial G_{mn}(k,k')}{\partial t} + H_{\rm WS}G_{mn}(k,k') = \delta(k-k')\delta(t-t'). \tag{2.40}$$

Upon performing a Fourier transformation, frequency-dependent Green's function can be derived in the Lehmann spectral representation

$$G^{(\omega)}_{mn}(k,k') = \sum_p \frac{\psi^{(p)}_{mnk}\psi^{(p)*}_{mnk'}}{E^{(p)}_{mn} - \hbar\omega}. \tag{2.41}$$

Different orders of density matrix elements can be obtained from Eqs. (2.39)-(2.41). The zeroth order is defined as $\rho^{(0)}_{lnk} = f^{(0)}_{nk}\delta_{ln}$, for which there is no external perturbation in the system. Thus, $f^{(0)}_{nk}$ is the population of band n. Knowing the zeroth order, the first order is obtained using the harmonic behavior of both density matrix and optical fields, i.e., $\rho^{(1)}_{mnk} = 1/2(\rho^{(\omega)}_{mnk}e^{-i\omega t} + \rho^{(\omega)*}_{mnk}e^{i\omega t})$ and $F_t = 1/2(F_\omega e^{-i\omega t} + F^*_\omega e^{i\omega t})$

$$\rho^{(\omega)}_{mnk} = -eF_\omega\bar{\delta}_{mn}\int G^{(\omega)}_{mn}(k,k')\Omega_{mnk'}f^{(0)}_{nmk'}dk', \tag{2.42}$$

where $f^{(0)}_{nmk}$ is the population difference between bands n and m. For obtaining this equation, a cold and clean system is considered, i.e., $df^{(0)}_{nk}/dk \approx 0$. Upon performing another iteration in Eq. (2.39), the second-order density matrix elements can be derived using the harmonic behavior of density matrix elements, i.e., $\rho^{(2)}_{mnk} = 1/4(\rho^{(2\omega)}_{mnk}e^{-2i\omega t} + \rho^{(2\omega)*}_{mnk}e^{2i\omega t} + \rho^{(\rm DC)}_{mnk})$

$$\begin{aligned} \rho^{(2\omega)}_{mnk} = -e^2F^2_\omega\int G^{(2\omega)}_{mn}(k,k')\Bigg[i\int\Bigg\{G^{(\omega)}_{mn}(k',k'')\Omega_{mnk''}f^{(0)}_{nmk''}\bar{\delta}_{mn}dk''\Bigg\}_{;k'} + \\ \sum_l\Bigg\{\Omega_{lnk'}\bar{\delta}_{ln}\int G^{(\omega)}_{ln}(k',k'')\Omega_{mlk''}f^{(0)}_{lmk''}\bar{\delta}_{ml}dk'' \\ -\Omega_{mlk'}\bar{\delta}_{ml}\int G^{(\omega)}_{ml}(k',k'')\Omega_{lnk''}f^{(0)}_{nlk''}\bar{\delta}_{ln}dk''\Bigg\}\Bigg]dk'. \end{aligned} \tag{2.43}$$

Non-diagonal density matrix elements (ρ_{mnk}, $m \neq n$) correspond to the coherence between bands m and n, whereas diagonal elements (ρ_{nnk}) are the population of band n. Using Eq. (2.39) for diagonal elements, the first order is $f^{(\omega)}_{nk} = 0$ and the second order is

$$f^{(2\omega)}_{nk} = -\frac{e^2 F^2_\omega}{\hbar\omega} \sum_l \left\{ \Omega_{lnk} \int G^{(\omega)}_{nl}(k,k') \Omega_{nlk'} f^{(0)}_{lnk'} \bar{\delta}_{nl} dk' \right.$$
$$\left. -\Omega_{nlk} \int G^{(\omega)}_{ln}(k,k') \Omega_{lnk'} f^{(0)}_{nlk'} \bar{\delta}_{ln} dk' \right\}. \tag{2.44}$$

The expectation value of any physical observable X is obtainable using the density matrix via $\langle \hat{X} \rangle = \mathrm{Tr}(\hat{\rho}\hat{X})$. Therefore, the expectation value of the induced current is

$$j(t) = -\frac{e}{\pi m} \sum_{mn} \int p_{nmk} \rho_{mnk} dk. \tag{2.45}$$

The Fourier transformation for the first and second orders of the current is $j^{(1)}(t) = 1/2(j(\omega)e^{-i\omega t} + j^*(\omega)e^{i\omega t})$ and $j^{(2)}(t) = 1/4(j(2\omega)e^{-2i\omega t} + j^*(2\omega)e^{2i\omega t} + j_{(\mathrm{DC})})$, respectively. The linear and second-order nonlinear parts of the response function, which in this case is the optical conductivity can be obtained via expressions $j(\omega) = \sigma_1(\omega)F_\omega$ and $j(2\omega) = \sigma_2(\omega)F^2_\omega$, respectively. To simplify the optical conductivity expressions, the following WS notation is introduced

$$P^{(p)}_{mn} = \int \psi^{(p)}_{mnk} p_{mnk} dk, \; O^{(p)}_{mn} = \int \psi^{(p)*}_{mnk} \Omega_{mnk} f^{(0)}_{nmk} dk,$$
$$Q^{(pq)}_{mn} = \int \psi^{(q)*}_{mnk} (\psi^{(p)}_{mnk})_{;k} dk, \; M^{(pq)}_{mn} = \int \psi^{(q)*}_{mnk} (\psi^{(p)}_{mnk}) \Omega_{mnk} dk, \tag{2.46}$$

Then, the linear optical conductivity is

$$\sigma_1(\omega) = \frac{e^2}{\pi m} \sum_{\substack{m,n \\ m \neq n}} \sum_p \frac{P^{(p)}_{nm} O^{(p)}_{mn}}{E^{(p)}_{mn} - \hbar\omega}. \tag{2.47}$$

For the second-order nonlinear conductivity, two expressions can be obtained

$$\sigma^{(eeie)}_2(\omega) = \frac{ie^3}{\pi m} \sum_{\substack{m,n \\ m \neq n}} \sum_{p,q} \frac{P^{(p)}_{nm} O^{(q)}_{mn} Q^{(pq)}_{mn}}{(E^{(p)}_{mn} - 2\hbar\omega)(E^{(q)}_{mn} - \hbar\omega)}. \tag{2.48}$$

$$\sigma^{(iiee)}_2(\omega) = \frac{e^3}{\pi m} \sum_{\substack{m,n,l \\ m \neq n, n \neq l, m \neq l}} \sum_{p,q} \left\{ \frac{P^{(p)}_{nm} O^{(q)}_{ml} M^{(pq)}_{ln}}{(E^{(p)}_{mn} - 2\hbar\omega)(E^{(q)}_{ml} - \hbar\omega)} \right.$$
$$\left. - \frac{P^{(p)}_{nm} O^{(q)}_{ln} M^{(pq)}_{ml}}{(E^{(p)}_{mn} - 2\hbar\omega)(E^{(q)}_{ln} - \hbar\omega)} \right\}. \tag{2.49}$$

2.4.3 Two-dimensional semiconductors

In this section, a simple method for extending one-dimensional optical response expressions obtained in Sec. 2.4.2 to two-dimensional semiconductors is introduced. The DC field is considered in the x-direction F^{x}_{DC}. Since the k-space is a two-dimensional grid of k-points for these systems and the DC field is taken along the x-direction, for each k_y-point, obtained expressions in Eqs. (2.47)-(2.49) are valid, where integrations in Eq. (2.46) are performed in the k_x-direction. Hence, the linear optical conductivity for two-dimensional systems can be obtained by performing a k_y-integration in Eq. (2.47) as follows

$$\sigma_1(\omega) = \frac{e^2}{\pi m} \sum_{k_y} \sum_{\substack{m,n \\ m\neq n}} \sum_{p} \frac{P^{(p)}_{nmk_y} O^{(p)}_{mnk_y}}{E^{(p)}_{mnk_y} - \hbar\omega}. \tag{2.50}$$

Similarly, for the second order nonlinear conductivity

$$\sigma_2^{(eeie)}(\omega) = \frac{ie^3}{\pi m} \sum_{k_y} \sum_{\substack{m,n \\ m\neq n}} \sum_{p,q} \frac{P^{(p)}_{nmk_y} O^{(q)}_{mnk_y} Q^{(pq)}_{mnk_y}}{(E^{(p)}_{mnk_y} - 2\hbar\omega)(E^{(q)}_{mnk_y} - \hbar\omega)}. \tag{2.51}$$

$$\sigma_2^{(iiee)}(\omega) = \frac{e^3}{\pi m} \sum_{k_y} \sum_{\substack{m,n,l \\ m\neq n, n\neq l, m\neq l}} \sum_{p,q} \left\{ \frac{P^{(p)}_{nmk_y} O^{(q)}_{mlk_y} M^{(pq)}_{lnk_y}}{(E^{(p)}_{mnk_y} - 2\hbar\omega)(E^{(q)}_{mlk_y} - \hbar\omega)} - \frac{P^{(p)}_{nmk_y} O^{(q)}_{lnk_y} M^{(pq)}_{mlk_y}}{(E^{(p)}_{mnk_y} - 2\hbar\omega)(E^{(q)}_{lnk_y} - \hbar\omega)} \right\}. \tag{2.52}$$

Chapter 3

Summary of results

This chapter presents results in this PhD project and discusses them. Most of the results can be found in the papers at the end of the thesis. First, the electronic structure of CNT-carbyne systems and graphene nanoribbons in papers ?? and ?? will be presented. Then, results of independent-electron optical response from papers ??, ?? and ?? will be presented and discussed. Next, results of excitonic effects on the optical response of CNT-carbyne systems from paper ?? will be discussed. Finally, DC fields effects on the optical response of one- and two-dimensional semiconductors from papers ?? and ?? will be presented.

3.1 Electronic structure

3.1.1 Hybrid CNT-carbyne systems

For systems consisting carbyne encapsulated inside single-walled CNTs in this thesis, density functional theory (DFT) and tight-binding (TB) are used to calculate their band structure. First, the band structure of hybrid (8,0) and (10.0) CNT-carbyne systems is obtained using DFT. Then, the DFT band structure is used to fit the TB band structure and obtain TB parameters. For calculating the band structure, it is necessary to define the unit cell of the hybrid system. There is a mismatch between the CNT unit cell (0.426 nm [21]) and the carbyne unit cell (0.256 nm [25]). Therefore, a supercell consisting five unit cells of carbyne and three unit cells of CNT is chosen with the length of 1.278 nm, resulting in a marginal mismatch of 0.16% between unit cells of the two subsystems. For the compensation of this mismatch, carbyne system is compressed in size to match the size of 1.278 nm. Then, eigenstates of two mentioned hybrid systems are calculated using the ABINIT package [141–144] with the Perdew-Burke-Ernzerhof generalized gradient approximation functional [145].

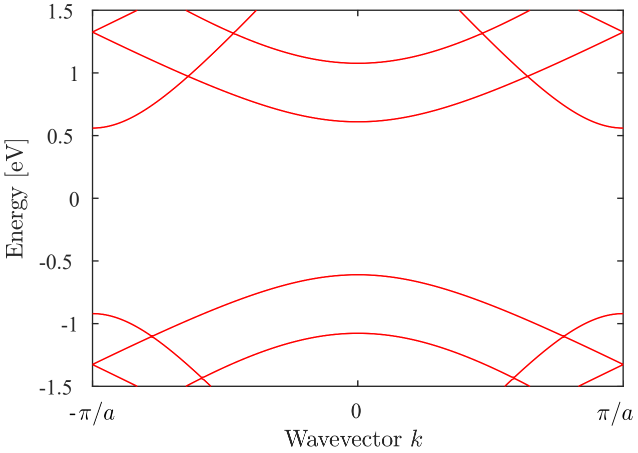

Fig. 3.1: Nearest neighbor TB band structure of (8,0) CNT-carbyne system without band hybridization.

The TB method enables one to obtain the electronic structure for a denser k-points choice with much less computational costs compared to DFT. First, two subsystems in (8,0) and (10,0) hybrid CNT-carbyne systems are considered without any interaction, and their band structure is obtained using the nearest neighbor TB method. In this model, single π-orbital for CNT and two perpendicular π-orbitals for carbyne are considered. For obtaining TB parameters by fitting the TB band structure against that of the DFT method, the electron-hole effective mass at high-symmetric k-points of the DFT band structure is calculated, then the TB parameters at those k-points are tuned to obtain similar effective masses. As results, the hopping parameters for (8,0) CNT-carbyne system are $\gamma_{\mathrm{CNT}} = 2.6$ eV for carbon-carbon bonds in CNT, as well as $\gamma^1_{\mathrm{car.}} = 3.56$ eV and $\gamma^2_{\mathrm{car.}} = 4.3$ eV for single and triple bonds of carbyne, respectively. For (10,0) CNT-carbyne system, the hopping parameters are similar to the (8,0) CNT-carbyne, except $\gamma^2_{\mathrm{car.}} = 4.15$ eV. Figure 3.1 shows the band structure of (8,0) CNT-carbyne system without considering interactions between two subsystems.

Interactions between CNT and carbyne systems in the energy range close to the band gap are obtained by hybridizing the first conduction band of CNT E_{CNT} with that of carbyne $E_{\mathrm{car.}}$, using the k-independent hybridized parameter h via the following determinant

$$\begin{vmatrix} E_{\mathrm{CNT}} - E & h \\ h & E_{\mathrm{car.}} - E \end{vmatrix} = 0,$$

Eigenvalues of this equation are $E_{\pm} = (E_{\mathrm{CNT}} + E_{\mathrm{car.}})/2 \pm ((E_{\mathrm{CNT}} - E_{\mathrm{car.}})^2 +$

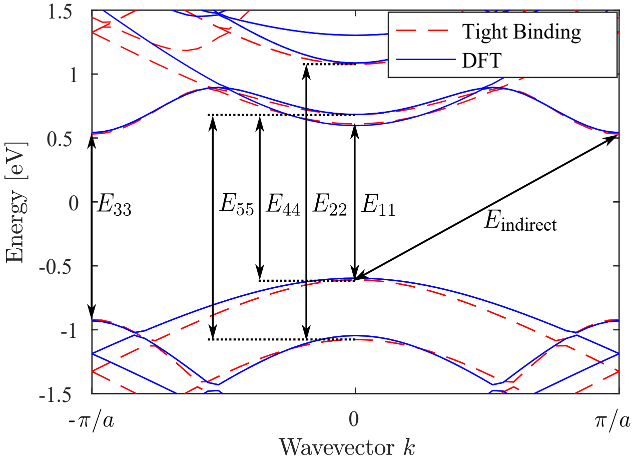

Fig. 3.2: Band structure of hybrid (8,0) CNT-carbyne system calculated by the DFT and TB methods. Arrows are different possible transitions around the band gap of the system.

$4h^2)^{1/2}/2$. The hybridized parameter $h = 0.16$ eV is also obtained from fitting the TB band structure against that of the DFT method. (8,0) CNT-carbyne band structure using DFT and fitted TB is shown in Fig. 3.2. The TB band structure has a good agreement with that of the DFT method, especially in the high-symmetric k-pints. $E_{11} = 1.22$ eV and $E_{22} = 2.15$ eV are energies resulting from the transitions between valence and conduction bands of isolated (8,0) CNT, and $E_{33} = 1.48$ eV is obtained from isolated carbyne. Hybridization of CNT and carbyne systems results in two extra transitions $E_{44} = 1.29$ eV and $E_{55} = 1.76$ eV in the energy region around the band gap. Moreover, Hybrid (8,0) CNT-carbyne system has an indirect band gap with the energy of $E_{\text{indirect}} = 1.17$ eV. It is noteworthy to mention that $E_{11} \approx 0.6$ eV in our DFT calculation. It has been shown that a quasi-particle GW correction can open the band gap of (8,0) CNT up to 1.8 eV [146]. Here, a scissors shift of 0.6 eV is applied to the DFT band gap, yielding the agreement between the TB and DFT band gap energy.

With a similar method for (10,0) CNT-carbyne system, transition energies are $E_{11} = 0.91$ eV, $E_{22} = 1.99$ eV, $E_{33} = 1.18$ eV, $E_{44} = 1.29$ eV, $E_{55} = 1.83$ eV and $E_{\text{indirect}} = 0.52$ eV.

3.1.2 Graphene nanoribbons in transversal DC fields

In this section, the band structure of narrow armchair graphene nanoribbons, i.e., AGNR-3 and AGNR-9 is calculated with and without the effect of applying DC fields along the perpendicular direction of the GNRs long-axis. Here, AGNR-n_d notation is used, which n_d is the number of carbon-carbon dimer

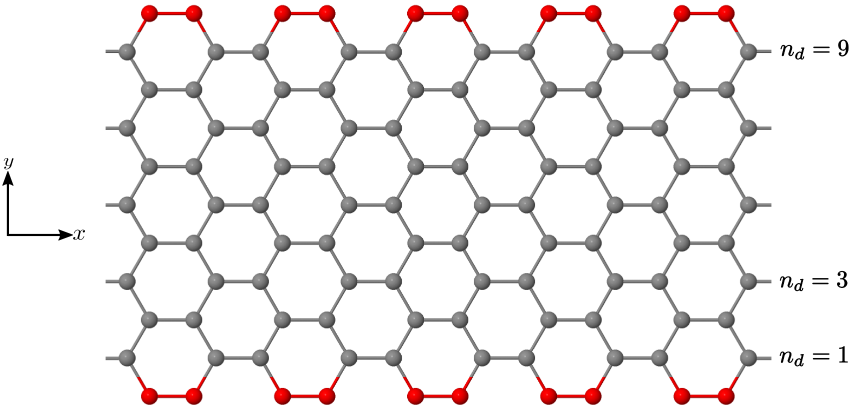

Fig. 3.3: Atomic structure of AGNRs up to $n_d = 9$ rows of carbon atoms (gray atoms), which chemical edge bonds are saturated with hydrogen atoms (red atoms).

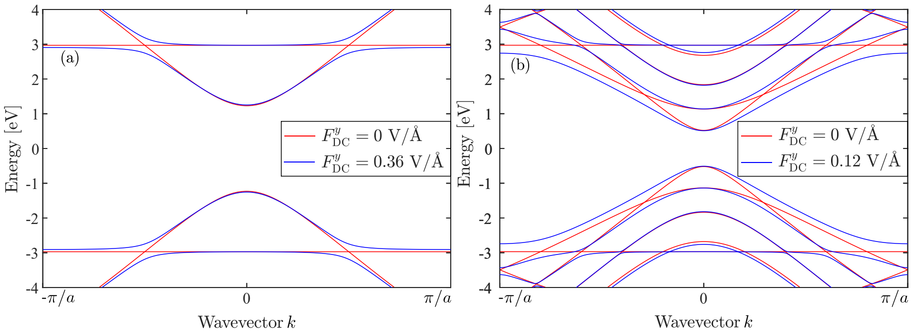

Fig. 3.4: Band structure of (a) AGNR-3 and (b) AGNR-9 with and without transversal DC field F_{DC}^{y}.

bonds in the structure, and edge carbon atoms are passivated by hydrogen atoms as shown in Fig. 3.3. Similar to CNT-carbyne systems, the nearest neighbor TB method is used for calculations, considering single π-orbital per atomic site. First, the band structure of AGNR-3 and AGNR-9 is calculated without the presence of external electrostatic fields. Then, $F_{\mathrm{DC}}^{y} = 3.6$ V/nm for AGNR-3 and $F_{\mathrm{DC}}^{y} = 1.2$ V/nm for AGNR-9 is applied to calculate their electronic band structure. The spectra in Fig. 3.4 show that including external transversal DC fields results in lifting degeneracies in the band-crossing points, which is the result of diagonal DC field energy terms eyF_{DC}^{y} in the Hamiltonian matrix. Changes in the band structure depend on the width of AGNRs and the intensity of the DC field. For a fixed DC field strength, the effect of DC fields in wider AGNRs is more prominent, due to the larger dipole moment along the width of these structures. Hence, larger DC field strength is used for AGNR-3

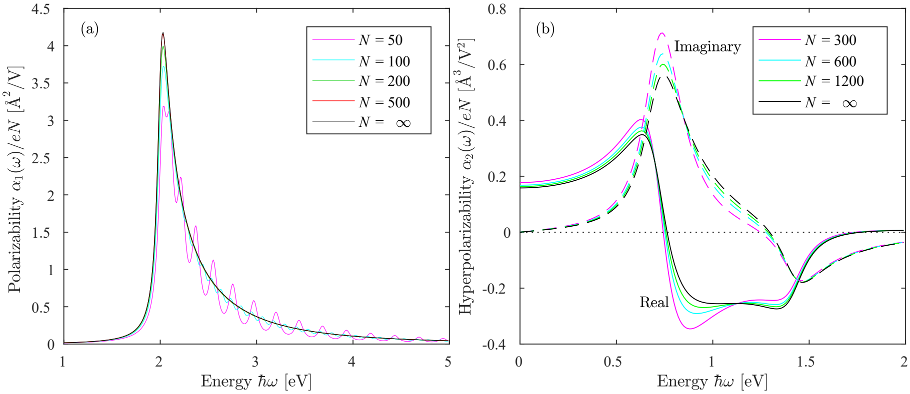

Fig. 3.5: (a) The imaginary part of the linear polarizability of polyacetylene and (b) real and imaginary parts of second-order nonlinear polarizability of polymethineimine, considering both finite and infinite lengths.

compared to AGNR-9 to obtain considerable changes in the band structure of this system.

3.2 Independent-electron optical response

This section presents the optical response of semiconducting carbon-based chains, graphene nanoribbons and sheets, as well as CNT-carbyne systems under external optical fields perturbation and neglecting many-body effects. Note that the long-axis of studied systems is taken along the x-axis and the optical response is calculated for optical fields polarized along this axis. Diagonal elements of the linear and nonlinear optical response tensors are considered, i.e., xx and xxx components for the linear and second-order nonlinear tensors, respectively.

3.2.1 One-dimensional carbon-based atomic chains

The optical response of finite and infinite polyacetylene and polymethineimine chains as shown in Fig. 1.1 are calculated using the quantum perturbation theory in paper **??**. Choosing TB parameters 0, -2 eV and -3 eV for on-site energy, single- and double-bond hopping energy, respectively, results in the optical band gap of 2 eV for polyacetylene. For polymethineimine chains, TB parameters are 0.5 eV, -2 eV and -2.5 eV, and the optical band gap is 1.41 eV. In Fig. 3.5, the linear and nonlinear polarizability α per unit cells number N of polyacetylene and polymethineimine chains are plotted, using the calculation methods in Sec. 2.2.1 for finite and Sec. 2.2.2 for infinite systems. With increasing the length of the finite system, the response of finite systems converges to

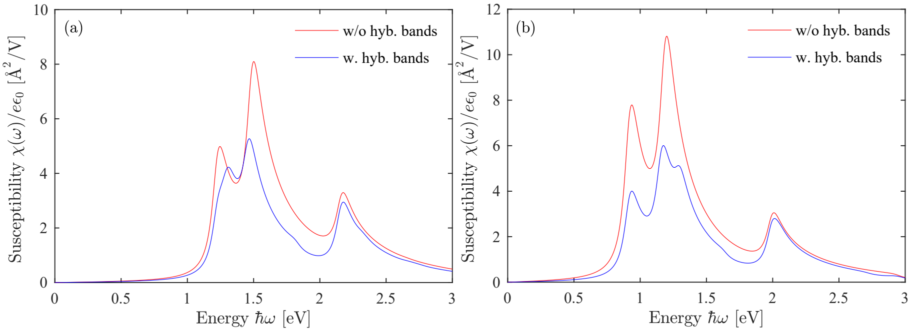

Fig. 3.6: The imaginary part of the linear optical susceptibility in the single-electron pictures for (a) (8,0) CNT-carbyne and (b) (10,0) CNT-carbyne, with and without interactions between CNT and carbyne systems.

that of infinite systems. In Fig. 3.5 (a), the major peak at 2 eV corresponds to electron transitions with absorbing photons with the energy of the band gap. Also, the response for the $N = 50$ system shows noticeable oscillations because of the energy difference between valence and conduction states are much larger than the broadening energy. The broadening is taken as $\hbar\Gamma = 50$ meV throughout the calculations in this thesis, except the obtained result for the nonlinear polarizability of polymethineimine in Fig. 3.5 (b), which is taken as $\hbar\Gamma = 100$ meV. With increasing the length of the system, the energy difference between valence and conduction states gets smaller and results in the vanishing oscillation peaks for long chains. Polyacetylene chain in this study has inversion symmetry, so there is no even-order nonlinear optical response for this system. For this reason, polymethineimine chain is chosen to calculate the second-order nonlinear polarizability instead. The imaginary parts of the spectra in Fig. 3.5 (b) show two distinct resonances at 1.41 eV and 0.705 eV, which are one- and two-photon resonances with the energy of the band gap, respectively.

3.2.2 CNT-carbyne systems

Both CNT and carbyne systems are optically very active materials because of their one-dimensional nature. Hence, the optical response of CNTs with various size and chirality are extensively studied theoretically and experimentally [59, 63–65]. Unlike CNTs, isolated long carbyne chains are not stable materials to study their optical response. It has been recently shown that the encapsulation of carbyne chains inside CNTs provide a good medium to grow long carbyne chains [25]. Therefore, this encapsulation produces new hybrid systems, which reflects the properties of isolated CNT and carbyne systems, as well as interactions between them. Based on the electronic structure of two

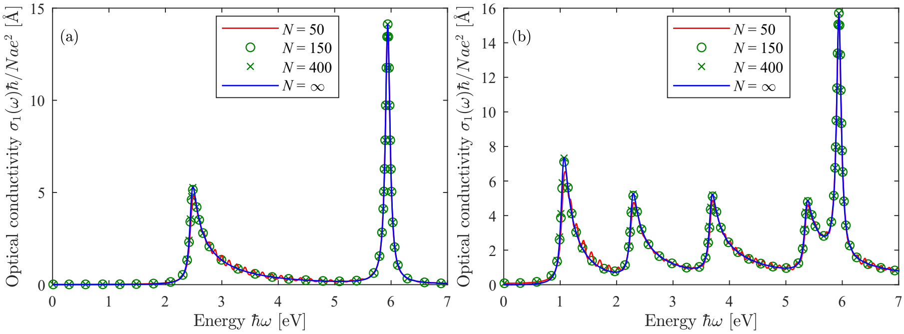

Fig. 3.7: The real part of the linear optical conductivity of (a) AGNR-3 and (b) AGNR-9, for finite systems with $N = 50 - 400$ unit cells and infinite systems $N = \infty$.

hybrid CNT-carbyne systems in Sec. 3.1.1, the single electron optical response of these systems are calculated using the method in Sec. 2.2.2. Figure 3.6 shows the imaginary part of the linear optical susceptibility χ from Eq. (2.24) for both (8,0) and (10,0) CNT-carbyne systems. The red and blue curves are the linear optical susceptibility for CNT and carbyne systems without and with interactions between them, respectively. Despite a relatively large distance between CNT and carbyne systems, the interaction between these two systems causes considerable changes in the optical response, in which the height of peaks are decreased and new peaks are introduced in the spectra. These peaks are explainable by looking into the band structure of (8,0) CNT-carbyne system in Fig. 3.2. Without the interaction, there are three peaks, which correspond to the transitions with energies E_{11}, E_{22} and E_{33}. Including the interaction introduces two more optical transitions E_{44} and E_{55} and results in extra features in the blue curves. Both (8,0) and (10,0) CNT-carbyne systems have an indirect band gap (E_{indirect}), which in our considered conditions (without external heat and phonon contributions) are optically inactive.

3.2.3 Graphene nanoribbons and sheet

Obtaining the optical response of GNRs have attracted a lot of attention in the past two decades, due to the one-dimensional nature of these materials. Figure 3.7 shows the real part of the linear optical conductivity for AGNR-3 and AGNR-9 per length Na, where N is the number of unit cells and k-points for finite and infinite systems, respectively. The figure is plotted for AGNRs with various lengths from $N = 50$ unit cells to $N = 400$, using the dipole moment formalism introduced in Sec. 2.2.1, and $N = \infty$ using the momentum matrix elements explained in Sec. 2.2.2, in which the equations are converted to the optical conductivity σ instead of the optical susceptibility χ. The real part of the linear optical conductivity shows the absorption of external photons

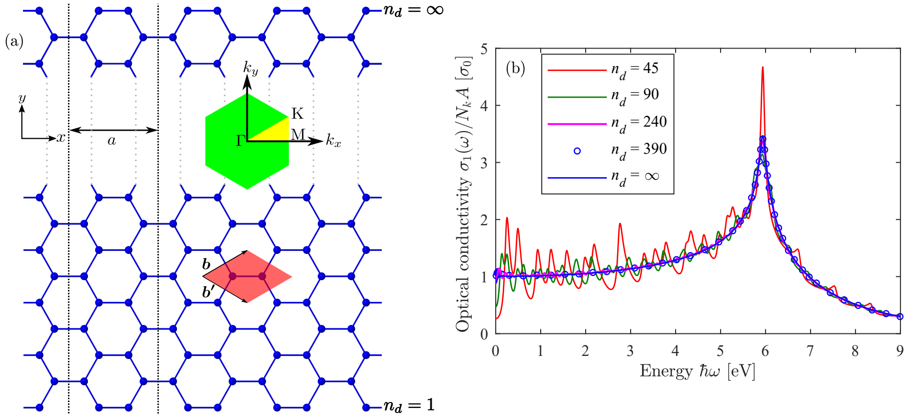

Fig. 3.8: (a) Atomic structure of AGNRs and graphene sheet. n_d is the row number of carbon-carbon dimer bonds, which $n_d = \infty$ corresponds to the graphene sheet. The area restricted between the dashed lines with the width of a corresponds to AGNRs unit cell. The green hexagon is the first Brillouin zone for graphene with Γ, K and M as high-symmetry k-points and the yellow triangle is the irreducible Brillouin zone. The red diamond is the unit cell of the graphene sheet with b and b' as unit vectors. (b) The real part of the linear optical conductivity for AGNRs with various width ($n_d = 45 - 390$) compared to the graphene sheet $n_d = \infty$ in the units of graphene DC conductivity σ_0.

by the system. Both AGNRs spectra show that the optical response of finite systems converges to that of the infinite systems in the limit of sufficiently long finite structures. The lowest energy peak in each spectrum corresponds to the absorption of external field photons with the energy of the band gap. Also, the large symmetrical peak is the result of the optical transition between the flat valence and conduction bands in Fig. 3.4. AGNR-9 spectrum has more peaks compared to AGNR-3, which is the result of more allowed optical transitions between valence and conduction bands for this system. Similar to the atomic chains in Sec. 3.2.1, short AGNRs such as the $N = 50$ system have oscillation peaks in their optical response, which is the reason of a large energy spacing between transitions compared to the chosen broadening for these sizes.

The optical response of graphene sheets has been already studied previously, e.g., Ref. [60]. It is expected that the optical response of sufficiently wide GNRs shows similar features as the two-dimensional graphene. Therefore, four various widths, i.e., AGNR-45, AGNR-90, AGNR-240, and AGNR-390 are chosen to calculate their linear optical conductivity with the similar method used for the narrow AGNRs. For two-dimensional graphene ($n_d = \infty$) as shown in Fig. 3.8 (a), a two-dimensional k-space is considered in the linear optical response equation in Sec. 2.2.2. The first Brillouin zone for such a two-dimensional k-space is shown as the green hexagon in Fig. 3.8 (a) with the yellow triangle as the irreducible Brillouin zone. Figure 3.8 (b) shows the real part of linear optical conductivity for wide AGNRs with various widths between $n_d = 45 - 390$ compared to the two-dimensional graphene $n_d = \infty$. The response is plotted in the graphene DC conductivity units $\sigma_0 = e^2/4\hbar$. In Fig. 3.8 (a), A is the area of the red diamond and hexagons between the two dashed lines for graphene and AGNRs, respectively. The spectra in Fig. 3.8 (b) show that increasing the width of AGNRs results in the convergence of their optical response to that of the two-dimensional graphene. As the optical field energy reduces, the response of graphene and wide AGNRs converges to a minimum value, corresponding to the DC optical conductivity of graphene σ_0. It should be noted that a small band gap of 0.02 eV is added to the graphene electronic structure (by adding on-site energies with opposite signs to the two sublattices) to avoid the divergence in the zero frequency of the optical field in our notation.

3.3 Excitonic effects in CNT-carbyne systems

In Sec. 3.2.2, the single-electron linear optical response of CNT-carbyne systems are presented and shown that the interactions between CNT and carbyne systems have remarkable effects in the optical response. Thus, it is expected to obtain remarkable excitonic effects in hybrid CNT-carbyne systems, as well. There are different exciton pairs in the hybrid systems, i.e., electrons and holes on isolated CNT and carbyne systems, as well as electrons on CNT and holes on carbyne or vice versa. Here, excitonic effects on the electronic structure and the optical response of hybrid (8,0) and (10,0) CNT-carbyne systems are calculated, using the Bethe-Salpeter equation (BSE) introduced in Sec. 2.3.1 and the Wannier method presented in Sec. 2.3.2.

For calculating excitonic effects using the BSE, the electron-hole Coulomb interaction from Eq. (2.31) is only considered and the exchange term Eq. (2.31) is ignored for the simplification. The electron-hole Coulomb interaction can be taken as an Ohno-type potential [124, 136]

$$v(\boldsymbol{r} - \boldsymbol{r}') = \frac{U}{\sqrt{(\frac{4\pi\varepsilon_0}{e^2})|\boldsymbol{r} - \boldsymbol{r}'|^2 + 1}},$$

where U is the Hubbard energy parameter and equals to 11.3 eV for π-orbitals in CNT and carbyne systems, which is the required energy for putting two electrons (holes) at a similar atomic site under the bare Coulomb potential. Then, the screening should be defined in the Coulomb expression. For hybrid CNT-carbyne systems in this study, which are normally synthesized in liquids such as water, it can be assumed that surrounding materials are mainly responsible for the Coulomb screening. Therefore, the screening is simply taken as the dielectric constant of the surrounding materials ε. In our calculations, the dielectric constant is chosen as $\varepsilon = 3.5$ [70].

system	transition	SET (eV)	E_b^{BS} (eV)	E_b^{W} (eV)	μ/m_e
(8,0) CNT-carbyne	CNT 1st	1.22	0.46	0.45	0.099
	CNT 2nd	2.15	0.47	0.45	0.095
	carbyne	1.48	0.42	0.40	0.028
	hyb. band	1.29	0.43	0.49	0.13
	indirect	1.17	0.21	0.16	0.003
(10,0) CNT-carbyne	CNT 1st	0.91	0.35	0.31	0.048
	CNT 2nd	1.99	0.49	0.48	0.2
	carbyne	1.18	0.38	0.37	0.023
	hyb. band	1.29	0.31	0.35	0.097
	indirect	0.54	0.18	0.15	0.003

Table 3.1: Summary of the single-electron and excitonic calculations of hybrid (8,0) and (10,0) CNT-carbyne systems. SET is the single-electron transition energy, E_b^{BS} and E_b^{W} are the exciton binding energy in the BSE and Wannier models, respectively and μ is the electron-hole reduced mass for each exciton divided by the electron mass m_e.

The Wannier approach can also be used to define exciton states and the optical response for hybrid CNT-carbyne systems. Unlike the BSE, in this method, the calculation is restricted to a single valence and conduction band pair. Therefore to obtain exciton states for the whole system, the Wannier equation (2.32) should be calculated separately for each band pair. Here, three different excitons are considered in the Wannier model in the low energy limit. First, excitons on CNTs, which both electrons and holes are on the CNT system. For these excitons, two band pairs as shown by transitions E_{11} and E_{22} in Fig. 3.2 are considered. Using Eq. (2.32), the basis function is taken as $\psi_m^W(\boldsymbol{r}) = (1/2\sqrt{2\lambda}\pi r_c)\mathbf{L}_m(|x|/\lambda)exp(-|x|/2\lambda)$, where $\lambda = 1.25$, r_c is the radius of the CNT system, $\mathbf{L}_m$ is Laguerre polynomials and x is the coordinate along the CNT axis. Also, the electron-hole potential is taken as $v(\boldsymbol{r}) = 1/\sqrt{4r_c^2\sin^2(z/2r_c) + x^2}$, where z is the the azimuthal coordinate of the CNT cylinder. Next, for electron-hole pairs on the carbyne system, the potential is considered as $v(\boldsymbol{r}) = 1/\sqrt{l^2 + x^2}$, which the length parameter l can be calculated from the self-energy of π-orbitals in carbyne and equals to 0.3 nm. Finally, if electrons are on CNT and holes are on carbyne or vice versa, a similar potential can be used with a small difference in the potential equation $v(\boldsymbol{r}) = 1/\sqrt{r_c^2 + x^2}$.

Exciton states can now be calculated using both the BSE and Wannier methods. Using these methods, the exciton binding energy and effective mass for different excitons are calculated and results are compared. Table 3.1 summarizes the calculation of exciton binding energies and electron-hole reduced masses in the (8,0) and (10,0) CNT-carbyne systems. CNT 1^{st} and 2^{nd} are transitions and exciton states for the first and second valence and conduction band pairs on CNTs. Hyb. band and indirect transitions are the result of

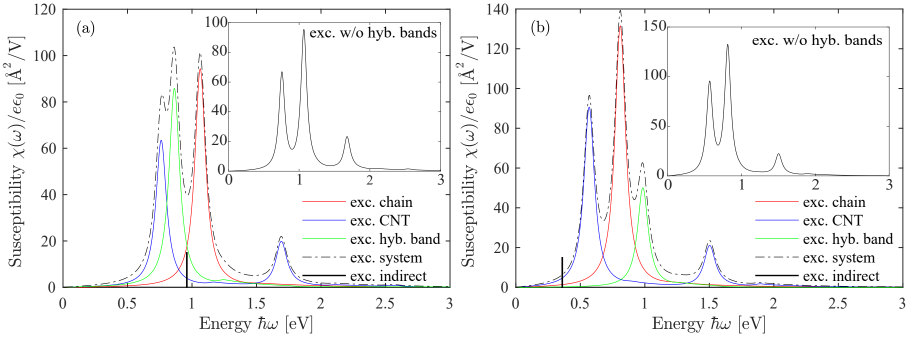

Fig. 3.9: The imaginary part of the excitonic linear optical susceptibility calculated by the BSE for (a) (8,0) CNT-carbyne and (b) (10,0) CNT-carbyne, using different colors for different excitonic contributions in the response, and the dashed line is the total response. The subset of each figure shows the excitonic optical susceptibility without the band hybridization between CNT and carbyne

interactions between CNT and carbyne as shown with E_{44} and E_{indirect} in Fig. 3.2, respectively. The numbers in the table show that exciton binding energies are considerable in hybrid CNT-carbyne systems. Comparing the results of the Wannier method with those of the BSE in the table, there are good agreements between these two methods, whereas it should be stressed that the BSE results are more accurate. In the following, the optical response of hybrid systems with the consideration of excitonic effects and interaction between two subsystems are discussed.

Figure 3.9 shows the imaginary part of the linear optical susceptibility for (8,0) and (10,0) CNT-carbyne systems calculated by the BSE. Subplots of the figure show the optical response without interactions between the two subsystems. In the energy range below 3 eV in Fig. 3.9 (a), three major peaks are visible, which peaks at 0.78 eV and 1.68 eV are the direct excitonic optical response of the first and second transitions in the (8,0) CNT system. The peak at 1.06 eV belongs to the excitonic optical response of isolated carbyne system. In the subset of Fig. 3.9 (b), (10,0) CNT peaks are at 0.56 eV and 1.5 eV and carbyne peak is at 0.8 eV. Comparing these results with non-excitonic results as shown as the red curves in Fig. 3.6, peaks are more symmetrical and red-shifted with the corresponding binding energies in Table 3.1. With including interactions between the two subsystems, the excitonic optical response is modified. In Fig. 3.9, two blue peaks belong to CNT systems. These peaks are similar to the CNT peaks in the non-interacting CNT-carbyne system as shown in the subsets of the figure. A new hybridized band as a result of the interaction between CNT and carbyne is introduced as shown in Fig. 3.2. This hybridized band results in the excitonic optical response as shown as the red and green curves in Fig. 3.9. The red curves at 1.06 eV for (8,0) and 0.8 eV for (10,0)

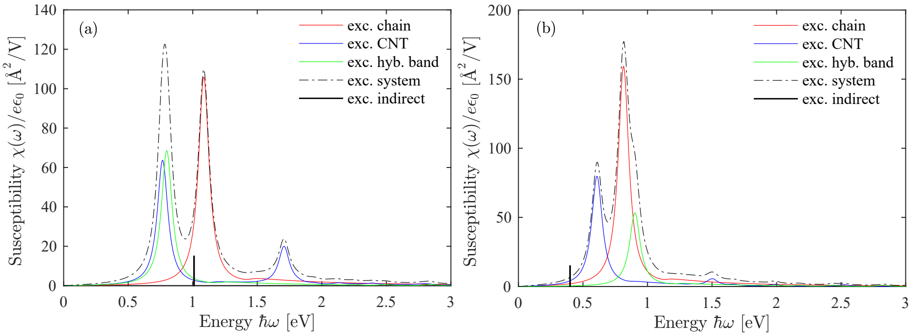

Fig. 3.10: The imaginary part of the excitonic linear optical susceptibility calculated by the Wannier method for (a) (8,0) CNT-carbyne and (b) (10,0) CNT-carbyne, using different colors for different excitonic contributions in the response, and the dashed line is the total response. The subset of each figure shows the excitonic optical susceptibility without the band hybridization between CNT and carbyne

CNT-carbyne are similar to the excitonic optical response of isolated carbyne in the subsets of the figure. The green curves are a new feature in the excitonic optical response of hybrid systems and correspond to the E_{44} transitions, in which electrons and holes are located on CNTs. Another remarkable feature of the interaction of two subsystems is the presence of spatially indirect excitons in the hybrid system as shown as the black bar in the figure at the energy of 0.96 eV and 0.36 eV for (8,0) and (10,0) CNT-carbyne, respectively. For these excitons, electrons are on CNT and holes are located on carbyne. Such excitons are optically inactive or dark excitons, i.e., they are not visible in the optical measurements. In Fig. 3.9, these dark excitons are illustrated to show their energy position compared to the bright excitons. For achieving bright excitons from these dark excitons, relaxation from initial bright excitations are needed, in which charge transfer occurs between two separated systems. Such charge transfers are unlikely because the large separation between CNT and carbyne systems makes these processes slower compared to electron-hole recombination processes in each subsystem. Despite the dark exciton in the (10,0) CNT-carbyne system in Fig. 3.9 (b) has the lowest energy, it is very unlikely to find electrons in this state without excessive external DC fields or temperatures.

Figure 3.10 shows the excitonic linear optical susceptibility calculated by the Wannier approach introduced in Sec. 2.3.2. As explained earlier, direct and indirect excitons are calculated using the basis function and chosen potential for each system. In the Wannier equation (2.32), it is necessary to obtain electron-hole reduced mass for each valence and conduction band pair, which in Table 3.1, the electron-hole reduced mass for different excitons are calculated. Solving the Wannier equation and plotting excitonic optical response in Fig. 3.10, results are in a good agreement with the BSE in Fig. 3.9. The

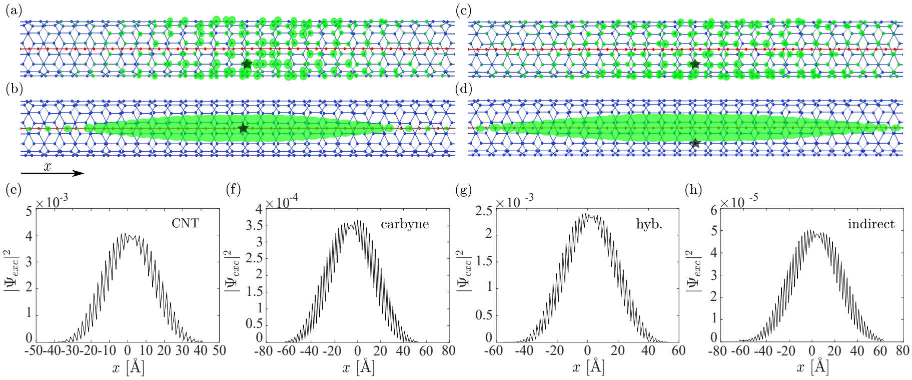

Fig. 3.11: The exciton probability distributions as a function of the electron position for different excitons, where holes are fixed at the center unit cell as shown by a black star: [(a) and (e)] the first exciton on the (8,0) CNT, [(b) and (f)] the exciton on carbyne inside the (8,0) CNT, [(c) and (g)] the exciton for the hybridized band of the (8,0) CNT-carbyne system, and [(d) and (h)] the indirect exciton on the (8,0) CNT-carbyne system.

peaks position and height are in comparable with those of the BSE calculation in Fig. 3.9.

The exciton probability distribution in the system shows that how the electron-hole interaction in the screened Coulomb potential affects this distribution. Here, the exciton probability distribution for four different exciton types in (8,0) CNT-carbyne system is shown in Fig. 3.11. The position of holes is fixed at the central unit cell of the system as shown by the black star in the figure, and the exciton probability function $|\psi_{exc}(\boldsymbol{r},\boldsymbol{r}')|^2$ is calculated using the exciton wave function obtained from the BSE. The electron probability distribution around the fixed hole for different excitons are shown in Fig. 3.11 (a)-(d). The figure shows that electrons are distributed over several unit cells of the system around the chosen hole position, in which the probability of finding electrons is higher around that position. The reason for this is that the Coulomb attraction between the electron and hole is stronger when the distance between them is smaller. Fig. 3.11 (e)-(h) shows the summation of the probabilities versus the electron position for each exciton. For direct excitons on the CNT, the total probability of finding electrons at each coordinate x comes from the summation of electron probabilities on a ring with an identical x value. For direct excitons on the carbyne system, there are two orbitals per atomic site. Therefore the total probability of each atomic site is the summation of the probability of two orbitals on that site. The figure shows that the total probability of electron is larger around the zeroth unit cell, where the hole is located on that cell. As the distance gets further from the hole position, the total electron probability gets smaller. Also, the probability depends on the exciton binding energy, in which a larger binding energy results in more

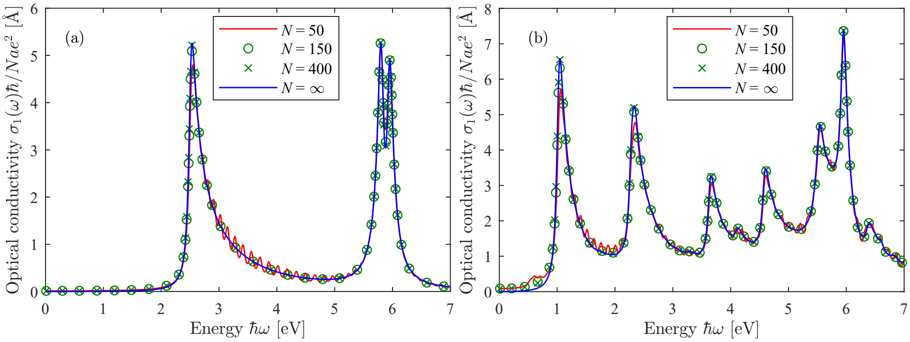

Fig. 3.12: The real part of the linear optical conductivity for (a) AGNR-3 under the transversal DC field $F^y_{\mathrm{DC}} = 3.6$ V/nm and (b) AGNR-9 under $F^y_{\mathrm{DC}} = 1.2$ V/nm, comparing various lengths of finite systems $N = 50 - 400$ unit cells with infinite systems $N = \infty$.

localized electrons around the hole position. It is also noteworthy to mention that the probability of electron distribution around the hole is not symmetric. The reason for this is the atomic positions in both CNT and carbyne systems are not symmetric around the chosen atomic site of the hole.

3.4 Transversal DC fields in graphene nanoribbons

The electronic band structure of AGNR-3 and AGNR-9 in Sec. 3.1.2 shows that applying transversal DC fields has considerable effects in their band structure. Therefore, these fields can modify the optical response of these systems. Before presenting the optical response results, a discussion of AGNR types is provided here. AGNRs are categorized into three types: AGNR-$3n_d$, AGNR-$(3n_d + 1)$ and AGNR-$(3n_d + 2)$, with n_d is an integer number showing the row number of carbon-carbon dimer bonds. In the TB method, AGNR-$3n_d$ and AGNR-$(3n_d+1)$ are semiconductors, while AGNR-$(3n_d+2)$ has the metallic behavior, i.e., there is no band gap for this type. All ZGNR types are also metallic in the TB approach. On the other hand, first principal approaches like DFT predict a small band gap for metallic GNRs in the TB method [48]. Moreover, the symmetrical properties are different for different types of GNRs. Under transversal DC fields, the inversion symmetry breaks for AGNR-$(3n_d + 1)$ and AGNR-$(3n_d + 2)$ types, while this symmetry is preserved for AGNR-$3n_d$ type. Since both AGNR-3 and AGNR-9 in this thesis are AGNR-$3n_d$ type, these structures keep their inversion symmetry under transversal DC fields. Therefore, even orders of the optical response for our chosen AGNRs with and without the presence of transversal DC fields are zero.

Now, the optical response of two selected AGNRs under transversal DC

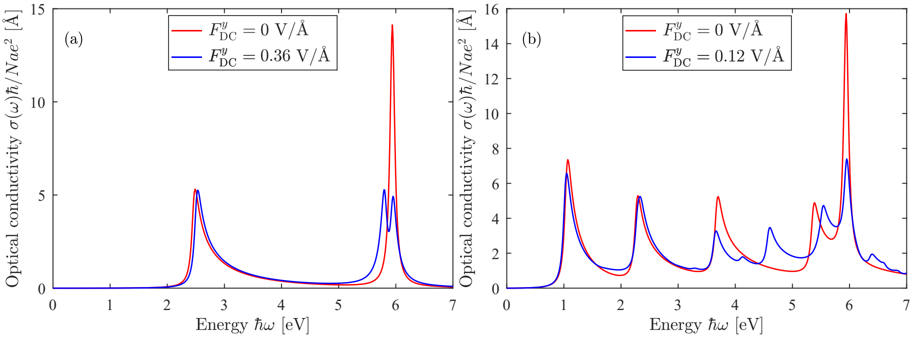

Fig. 3.13: The real part of the linear optical conductivity of infinite (a) AGNR-3 (b) AGNR-9, with and without applying the transversal DC field F^y_{DC}.

fields are calculated, considering various lengths of these systems. To this end, the method in Sec. 2.4.1 is used for calculating the linear optical conductivity for finite AGNR-3 under $F^y_{\mathrm{DC}} = 3.6$ V/nm and AGNR-9 under $F^y_{\mathrm{DC}} = 1.2$ V/nm taking 50, 150 and 400 unit cells, as well as infinitely long systems in Fig. 3.12. Similar to the non-DC results in Fig. 3.7, Fig. 3.12 shows that the optical response spectra for finite systems converge to those of infinite systems with increasing the length of finite structures.

Transversal DC fields effects in the optical response of AGNRs can be investigated by comparing the results in Fig. 3.12 with the non-DC optical response in Fig. 3.7. In Fig. 3.13, the optical conductivity of infinite AGNR-3 and AGNR-9 with and without transversal DC fields are presented. Both AGNRs show considerable changes in their optical response in the presence of DC fields. The changes are seen as new resonance peaks and modifications in the position and amplitude of some of the existing resonances. Modifications in the optical response can be understood from the changes of the band structure in Fig. 3.4 in the presence of the field, where F^y_{DC} changes the band structure and lifts the energy degeneracies in the band-crossing points. Also, the field slightly modifies the band gap energy of AGNRs.

3.5 Longitudinal DC fields in Semiconductors

This section presents the results of longitudinal DC fields effects on the linear and nonlinear optical response of one- and two-dimensional semiconductors calculated in papers **??** and **??**. For one-dimensional semiconductors, both finite and infinite polyacetylene chains and narrow AGNRs (AGNR-3 and AGNR-9) are considered to study the convergence of finite systems results to those of infinite ones in the limit of long finite systems. For two-dimensional semiconductors, the optical response of gapped graphene compared to wide AGNRs is

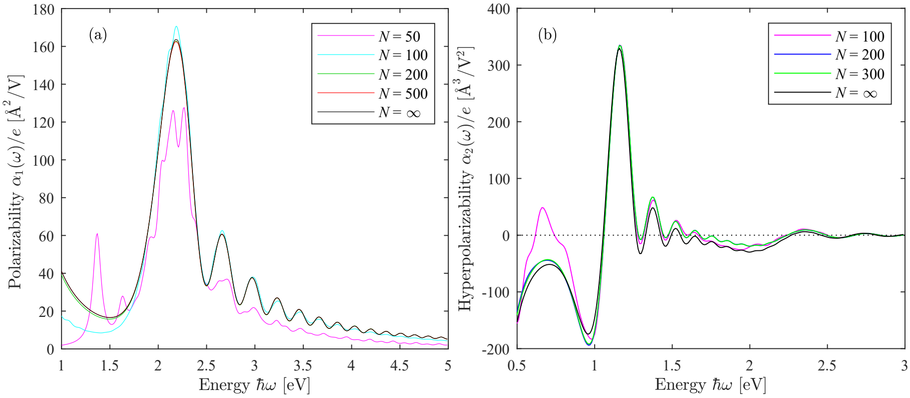

Fig. 3.14: The imaginary part of (a) linear and (b) second-order nonlinear polarizability of finite and infinite polyacetylene chain under the effect of longitudinal DC field $F_{\mathrm{DC}} = 0.2$ V/nm.

calculated.

Before providing the results, it is necessary to discuss charge transfer conditions under DC fields. In Fig. 2.1, it has been shown that an external DC field tilts the energy states of the system. For a finite system with the length L, if the DC field energy is larger than the band gap energy, i.e., $eF_{\mathrm{DC}}L > E_g$, the charge will be transferred from the ends of such a finite system. In such circumstances, the Fermi level crosses both valence and conduction bands. It should be noted that the DC field intensity must be strong enough to have charge transfer effects in such nanoscale semiconductors. Here, complications of the charge transfer in the optical response are avoided by restricting the DC filed energy to be smaller than the band gap $eF_{\mathrm{DC}}L < E_g$. Despite the condition $eF_{\mathrm{DC}}L > E_g$ is always valid for infinite systems and the charge will be transferred under any DC field, it is interesting to show that how infinite system formalism in k-space can predict finite systems behavior satisfying $eF_{\mathrm{DC}}L < E_g$. The reason for applying DC fields in infinite systems is that the calculation of the optical response for these systems are computationally much efficient compared to the calculations for finite systems, especially when there is a large number of atoms in their structure.

3.5.1 Polyacetylene chains

Polyacetylene chains have two atoms in their unit cell as shown in Fig. 1.1 (a), so in the nearest neighbor TB method, they are a two-band model of a semiconductor. Therefore, the method introduced in Sec. 2.4.2 can be simplified for these chains. For instance, a simplified version of the linear polarizability can be obtained from Eq. (2.47) using the relation between conductivity and polarizability via $\sigma(\omega) = -i\omega\alpha(\omega)$

$$\alpha_1(\omega) = \frac{ie^2}{\pi m\omega} \sum_p \frac{P_{vc}^{(p)} O_{cv}^{(p)}}{E_{cv}^{(p)} - \hbar\omega}.$$

Figure 3.14 (a) shows the imaginary part of the linear optical polarizability for polyacetylene chain under the longitudinal DC field $F_{\mathrm{DC}} = 0.2$ V/nm. The resonance peak at 2 eV in Fig. 3.5 is slightly blue-shifted under the field. The oscillatory resonances above the blue-shifted band gap peak are the result of transitions between Wannier-Stark (WS) states within valence and conduction bands of the chain. Also, there is a tail in the optical response below the band gap, which is the result of the tunneling across the band gap under the DC field as shown in Fig. 2.1. These Franz-Keldysh (FK) fingerprints, i.e., the oscillation peaks above and the optical response tail below the band gap can be explained by the Airy function behavior of the optical response in the effective mass model in Ref. [88]. Moreover, a considerable optical response is observable in the low energy limit $\hbar\omega < 1.5$ eV for long finite and infinite polyacetylene. This is, in fact, the artifact of the charge transfer in longer finite ($N > 100$) and infinite systems because the condition $eLF_{\mathrm{DC}} < E_g$ is not satisfied for these finite lengths. For infinite polyacetylene, such artifacts are obtainable by including intraband band pairs (v, v) and (c, c) in the above-mentioned polarizability equation.

Polyacetylene chains have central symmetry in their structure, so there is no second-order nonlinear optical response for these materials, whereas including DC fields in this system breaks the symmetry and electric field-induced second-order nonlinear optical response is expected. In Fig. 3.14 (b), the second-order nonlinear polarizability is calculated under the effect of $F_{\mathrm{DC}} = 0.2$ V/nm, using Eq. (2.48) introduced in Sec. 2.4.2. Since polyacetylene chains in this study have two bands, Eq. (2.49) is zero for these structures. The second-order nonlinear response has features similar to FK effects in the linear response, in which oscillation peaks after each one- and two-photon resonances are expected [117]. As Fig. 3.14 (b) illustrates, one- and two-photon resonances at 2 eV and 1 eV are seen, respectively. These resonances are followed by the oscillation peaks with different amplitudes and periods. The charge transfer artifact is also responsible for a huge optical response below 0.5 eV for long finite systems. Similar to the linear response, including (v, v) and (c, c) band pairs yields such artifacts for the infinite system. Moreover, as expected, finite system results converge to those of the infinite system with increasing unit cells number.

3.5.2 Narrow graphene nanoribbons

In this section, longitudinal DC fields effects on the optical response of two narrow GNRs, i.e., AGNR-3 and AGNR-9 are calculated. Transversal DC fields

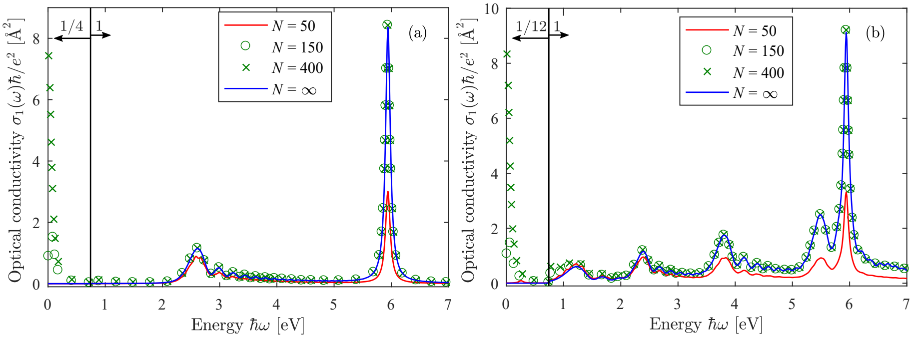

Fig. 3.15: The real part of the linear optical conductivity of (a) AGNR-3 (b) AGNR-9, considering various lengths of finite system $N = 50 - 400$ unit cells and infinite system $N = \infty$ under the longitudinal DC field $F^x_{\mathrm{DC}} = 0.1$ V/nm. Note that the low-energy parts of the spectra have been down-scaled.

effects in these systems have already been calculated in Sec. 3.4 and shown that strong fields are responsible for changes in the band structure and optical response of these materials. Applying longitudinal fields in these systems, similar to polyacetylene chains, results in breaking the band structure into localized WS energy states. Unlike polyacetylene which is a two-band model of a semiconductor, both chosen AGNRs are multiband systems, and the calculations are more complicated.

Equation (2.47) in Sec. 2.4.2 is used to calculated the linear optical conductivity for two selected narrow AGNRs in Fig. 3.15, considering the longitudinal DC field $F^x_{\mathrm{DC}} = 0.1$ V/nm. Each valence and conduction band pair with momentum-allowed optical transitions between them splits into WS states. Thus, oscillatory peaks are visible after each resonance peak for both AGNR-3 and AGNR-9 as a result of transitions between these WS states. Comparing this figure with Fig. 3.7, all peaks are blue-shifted for both AGNRs, which is similar to the obtained result for polyacetylene in Fig. 3.14 (a). Moreover, both AGNRs have an optical absorption tail below the band gap, which is the result of field-induced tunneling across the band gap under the DC field influence for these structures. The response of both finite AGNRs converges to that of infinite systems, as the length of the finite systems increases, which for $N = 150$ unit cells number, good agreement between finite and infinite results is observable.

The spectra in Fig. 3.15 are plotted from the zero external field energy to precisely discuss the low-energy behavior of the results. For finite systems with $N = 150$ unit cells and particularity for $N = 400$, there is a huge optical response in the low energy part of the spectra. This response is the result of charge transfer artifacts in our formalism for these structures because the DC field energy is larger than the band gap for these systems. Therefore, strong

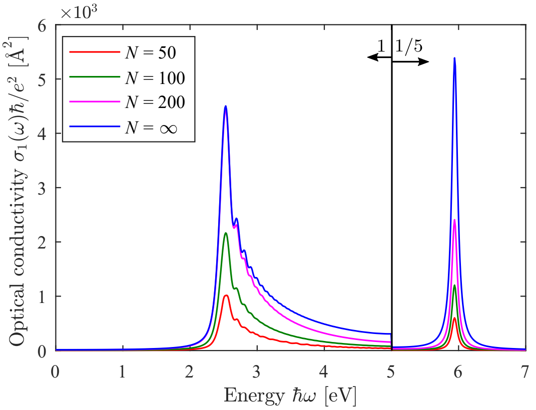

Fig. 3.16: The real part of the linear optical conductivity of AGNR-3, considering various lengths of finite system $N = 50 - 200$ unit cells and infinite system $N = \infty$ under the longitudinal DC field $F_{\mathrm{DC}}^{x} = 0.3$ V/nm. Note that above 5 eV, the spectra have been downscaled.

DC fields in these systems lead to the Fermi level crosses several valence and conduction states. Unlike the infinite polyacetylene in Fig. 3.14 (a), infinite AGNRs in Fig. 3.15 do not show any response in the low energy limit because intraband (v, v) and (c, c) contributions are neglected in the calculations of infinite AGNRs to avoid such non-physical charge transfer artifacts in the optical response.

Up until now, it has been shown that the infinite system modeling can predict finite systems optical response, and good agreements in the optical response of sufficiently long finite and infinite systems have been achieved. The remaining issue is that the charge will be transferred for long finite systems with the length L if their band gap energy is smaller than the DC field energy $eLF_{\mathrm{DC}} > E_g$. Therefore, for practical purposes, it is necessary to investigate how our infinite system modeling can predict finite systems optical response satisfying the condition $eLF_{\mathrm{DC}} < E_g$. In Fig. 3.15, it can be seen that $N = 50$ system satisfies the this condition because there is no charge transfer artifact in the low energy limit. For this finite system, infinite system result is not satisfactory enough, however, all the resonance peaks position is predicted correctly. Thus, it is expected that with decreasing the DC field intensity, longer finite system satisfying the condition $eLF_{\mathrm{DC}} < E_g$ can be studied to achieve a better convergence between finite and infinite results. Figure 3.16 shows the real part of the optical conductivity for AGNR-3 under $F_{\mathrm{DC}}^{x} = 0.3$ V/nm. The figure illustrates that decreasing the DC field intensity enables increasing the system length up to $N = 200$ unit cells satisfying $eLF_{\mathrm{DC}} < E_g$. These modifications result in a good agreement between $N = 200$ and infinite system results. Thus, it can be concluded that infinite system modeling is applicable for predicting

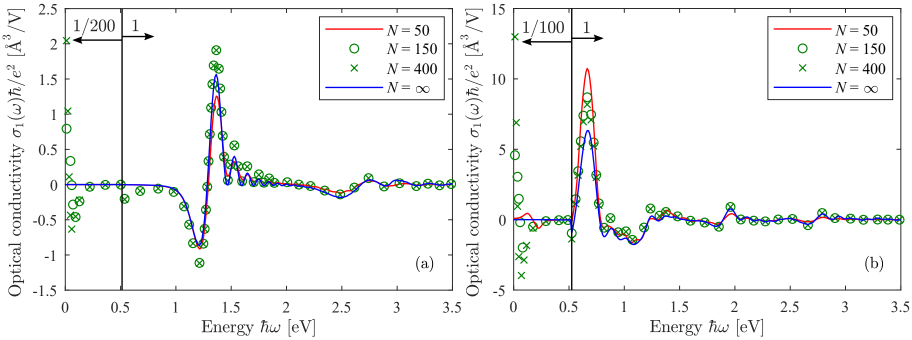

Fig. 3.17: The real part of the second-order nonlinear optical conductivity of (a) AGNR-3 (b) AGNR-9, considering various lengths of finite system $N = 50 - 400$ unit cells and infinite system $N = \infty$ under the longitudinal DC field $F^x_{\mathrm{DC}} = 0.1$ V/nm. Note that the low-energy parts of the spectra have been down-scaled.

finite systems behavior under the influence of strong longitudinal DC fields for practical relevance.

AGNRs are centrosymmetrical materials, which their even orders of nonlinear optical response are zero. Similar to polyacetylene chains, applying longitudinal DC fields breaks the center of symmetry and leads to the second-order nonlinear optical response. Equation. (2.48) in Sec. 2.4.2 is utilized for obtaining the second-order nonlinear optical conductivity for AGNR-3 and AGNR-9 under the effect of $F^x_{\mathrm{DC}} = 0.1$ V/nm in Fig. 3.17. For AGNR-3 in Fig. 3.17 (a), oscillatory features after one- and two-photon resonances are seen, which are similar to the features of polyacetylene chains and also in agreement with Ref. [117]. For AGNR-9 in Fig. 3.17 (b), there are more momentum-allowed optical transitions compared to AGNR-3, so oscillatory features of one- and two-photon resonances for each band pair are mixed and not distinguishable as AGNR-3. The result of both AGNRs shows that the most prominent response belongs to the two-photon resonance with the energy of the band gap of each system. Also in Fig. 3.17, considerable optical response close to the zero photon energy is seen, especially for $N = 150$ and $N = 400$ systems, which is the result of charge transfer artifacts similar to the linear case in Fig. 3.15. For infinite systems, such unphysical responses are not present because of omitting (v, v) and (c, c) band pairs in the calculation of Eq. (2.48).

3.5.3 Wide AGNRs and graphene sheet

It has been shown in Fig. 3.8 (b) that increasing the width of GNRs leads to the convergence of their optical response to that of two-dimensional graphene. In this section, the DC optical response of wide AGNRs compared to the two-dimensional graphene is calculated. For wide AGNRs, the similar method used

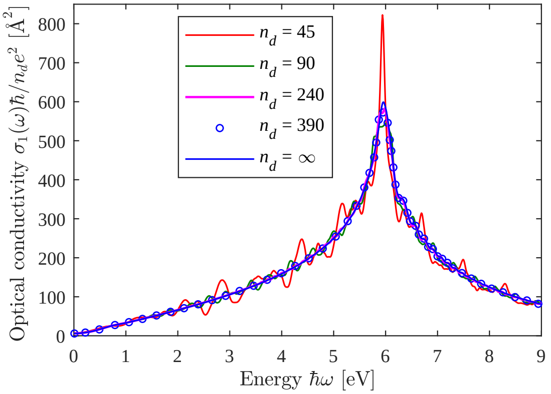

Fig. 3.18: The real part of the linear optical conductivity of AGNRs with the width of $n_d = 45 - 390$ carbon-carbon rows and the two-dimensional graphene $n_d = \infty$ under the longitudinal DC field $F^x_{\mathrm{DC}} = 0.1$ V/nm.

for narrow ones in the previous section is used, and for the graphene sheet, equations in Sec. 2.4.3 are employed. Again, the longitudinal DC fields $F^x_{\mathrm{DC}} = 0.1$ V/nm is applied in both wide AGNRs and the two-dimensional graphene to plot their linear optical conductivity spectra in Fig. 3.18 for AGNR-45, AGNR-90, AGNR-240, AGNR-390, and the graphene sheet (AGNR-∞). The factor of n_d for the graphene sheet is the number of k-points in the y-direction. The major response at 5.94 eV belongs to the optical transition with the energy of the Γ-point in the graphene Brillouin zone. This peak is followed by FK oscillations, which is similar to the results of one-dimensional semiconductors. In the calculation method in this thesis in agreement with Ref. [131], it has been shown that graphene bands are discretized into WS states, similar to one-dimensional semiconductors. Therefore, the oscillation peaks in graphene are the result of optical transitions between WS states located within valence and conduction bands. Below this energy point, the photon absorption between any momentum-allowed valence and conduction states and corresponding oscillations for each transition are mixed. In the case of graphene spectrum, a continuous response is achieved, which is the result of continuous absorption between valence and conduction states. In the case of wide AGNRs such as AGNR-240 and AGNR-390, at each k-point, the separation between energy states in different valence and conductions bands is very small compared to narrower AGNRs, which energy states of these wide AGNRs can be considered as continuous similar to graphene sheets. As the width of AGNR gets narrower like AGNR-90 and AGNR-45, the distance between energy states gets larger at each k-point and oscillatory features are prominent, however, these oscillations have no definite period because they are a mixture of different oscillations belong to different resonances.

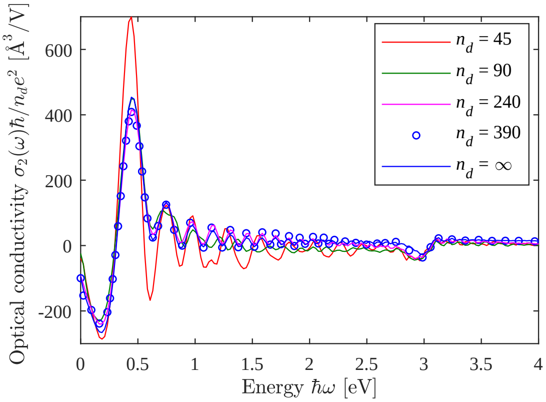

Fig. 3.19: The real part of the second-order nonlinear optical conductivity of AGNRs with the width of $n_d = 45-390$ carbon-carbon rows and two-dimensional graphene $n_d = \infty$ under the longitudinal DC field $F^x_{\mathrm{DC}} = 0.1$ V/nm.

Longitudinal DC fields break the central symmetry in wide AGNRs and two-dimensional graphene. Hence, the second-order nonlinear optical response of these systems can be calculated. In Fig. 3.19, the real part of the second-order nonlinear conductivity for the two-dimensional graphene and wide AGNRs from 45 to 390 rows of carbon-carbon bonds under the effect of the longitudinal DC field $F^x_{\mathrm{DC}} = 0.1$ V/nm is plotted. A dominant resonance below the optical field energy of 0.5 eV followed by the oscillatory resonances above that point is seen. This energy region belongs to one- and two-photon resonances between the K and M points in the graphene Brillouin zone. With increasing the energy toward 3 eV, oscillations get weaken and the oscillation period becomes non-definite, which can be a result of mixing of one- and two-photon resonances and their corresponding oscillations in this energy region. At the energy point of 2.97 eV, a distinct response is observed, which belongs to the two-photon resonance with the energy of the Γ-point in the graphene Brillouin zone. This resonance is followed by weak oscillations, which again because of the mixture of oscillations belong to other points of the Brillouin zone. Similar to the linear response in Fig. 3.17, wider AGNRs (AGNR-240 and AGNR-390) have a good agreement with the two-dimensional graphene, while in narrower AGNRs (AGNR-45 and AGNR-90), oscillatory features for the energy region between K and M points have non-definite periods. Furthermore, increasing the width of AGNR yields a better convergence to the two-dimensional graphene response.

Chapter 4

Conclusions

Electronic and optical properties of one-dimensional semiconductors differs considerably with their two- and three-dimensional counterparts. The main focus of this thesis has been to investigate the optical properties of one-dimensional semiconductors under the influence of external electrostatic fields and many-body excitonic effects.

Since long carbyne chains can be fabricated stably inside carbon nanotubes (CNTs) with the optimum distance of 0.338 nm between the inner wall of CNT and carbyne systems, the result is quasi-one-dimensional hybrid CNT-carbyne systems with unique electronic and optical properties. In this thesis, two hybrid systems have been considered, i.e., (8,0) and (10,0) CNT-carbyne, which both are a semiconductor and in the optimum radius range for growing carbyne systems. Then, a DFT method has been utilized to obtain the band structure for hybrid systems and tight-binding (TB) parameters by fitting the TB band structure against the DFT. Encapsulating carbyne inside CNT results in the interaction between two subsystems and the band structure of hybrid systems is modified compared to that of two isolated systems. Consequently, the single electron linear response of these hybrid systems are modified compared to isolated CNT and carbyne systems. Moreover, interactions between two subsystems have considerable effects in the excitonic states and optical response of hybrid systems. Exciton states can be formed as direct excitons, where electron and hole pairs are located on isolated CNT or carbyne systems, as well as spatially indirect excitons, which electrons are in CNT and holes are on carbyne systems or vice versa. Therefore, the excitonic optical response of hybrid systems is the combination of all direct and indirect excitons. Both Bethe-Salpeter and Wannier approaches have been used to calculate the exciton binding energy for different excitons and excitonic optical response. Obtained results have shown a considerable exciton binding energies in the system, which for direct excitons in CNTs, good agreements with previous studies has been achieved. Spatially indirect excitons are dark excitons, which due to the fast electron-hole recombinations in the optical processes, it is hard to populate these states. In the case of (10,0) CNT-carbyne system, the indirect exciton has the lowest transition energy in the system.

The presence of DC fields changes the electronic structure and optical response of materials, in which these changes depend on the structure, constitutional atoms, the direction and intensity of applied fields. In semiconductors, DC fields are responsible for considerable Franz-Keldysh (FK) effects, which field-assisted tunneling across the band gap results in the optical response tail below the band gap. Also, DC fields break the periodic band structure of semiconductors into localized Wannier-Stark (WS) states, which optical transitions occur between these states. In the case of atomic chains like polyacetylene and polymethineimine polymers in this thesis, DC fields along the long-axis of these systems are responsible for highly non-perturbative FK effects. For obtaining the optical response with and without DC fields effects, a nearest neighbor tight-binding model has been used to calculate the electronic structure of both finite and infinite polymers. For finite systems, the quantum perturbation theory has been used to calculate the linear and nonlinear optical response with and without the presence of DC fields, utilizing the dipole moment formalism in the calculation. For infinite systems, the quantum perturbation theory using momentum matrix elements has been employed for the optical response without DC fields. Under the effect of DC fields, a novel density matrix method has been developed to obtain WS states of the system and calculate the optical response. Results have shown that the optical response of finite systems converge to that of infinite ones when sufficiently large finite systems are considered. Also, FK effects in the linear optical response for polyacetylene chains have been observed, i.e., the presence of an optical response tail below and the oscillatory response above the band gap. Moreover, the broken symmetry of polyacetylene chains has yielded a considerable field-induced second-harmonic generation in these systems. Since calculations for infinite systems are performed in the k-space, for large finite systems resembling infinite structures, it is computationally much faster to obtain results for infinite systems.

In graphene nanoribbons (GNRs), the presence of DC fields parallel or perpendicular to the long-axis of GNR has different effects in the electronic structure and optical properties of these systems. For the perpendicular direction (transversal direction), strong DC fields lift the energy degeneracies and result in modifications of the band structure and optical response. These modifications depend on the field intensity and the width of GNR, in which for a fixed DC field intensity, the field effect is stronger in wider GNRs because of a larger induced dipole moment in these systems. The optical response of two armchair GNRs, i.e., AGNR-3 and AGNR-9 have been obtained for both finite and infinite lengths. In the limit of long finite systems, a good agreement between finite and infinite results has been achieved. DC fields can break the central symmetry and lead to the field-induced second-order nonlinear optical response. This symmetry is not broken for the chosen AGNRs in this study, which are the type AGNR-$3n_d$ with n_d as the row number of carbon-carbon bonds.

Similar to polyacetylene chains, DC fields in the parallel direction of the long-axis of GNR (longitudinal direction) are responsible for highly non-perturbative FK effects. Both AGNR-3 and AGNR-9 are multi-band semiconductors in the nearest neighbor TB model. Hence, in this thesis, a general method has been developed to calculate the optical response of multi-band infinite semiconductors. Comparative optical response results for finite and infinite AGNRs have shown a good agreement between long finite and infinite systems, which oscillatory resonances and optical response tail after and before every momentum-allowed transitions have been obtained. Moreover, due to the broken symmetry under DC fields, the second-order nonlinear optical response shows FK-type resonances after each one- and two-photon resonances for both AGNRs. Calculation of DC fields effects for infinite systems considerably reduces the computational costs compared to finite systems in AGNRs. This model can also reasonably predict the behavior of long finite systems without the charge transfer effect, for which DC field energies are smaller than the band gap energy.

GNRs structure and consequently the electronic and optical response converge to the two-dimensional graphene with increasing the width of GNR. The width of AGNRs has been increased from 45 to 390 carbon-carbon rows yielding a good agreement between sufficiently wide AGNRs and graphene sheets. For the optical response in the presence of DC fields, the one-dimensional method introduced for AGNRs has been extended to two-dimensional semiconductors to calculate the linear and nonlinear optical response of graphene sheets. The agreement between the optical response of wide AGNRs and the two-dimensional graphene has shown that the extended method for two-dimensional semiconductors is a capable model for predicting the optical response of wide one-dimensional semiconductors. The two-dimensional model has a benefit of decreasing the calculation time and computational resources needed for obtaining the results for wide one-dimensional semiconductors.

References

[1] L. S. Pan and D. R. Kania, *Diamond : electronic properties and applications*, (Springer Science+Business Media, New York, 1995).

[2] B. T. Kelly, *Physics of graphite*, (Applied Science, United Kingdom, 1981).

[3] N. Ashcroft and N. Mermin, *Solid State Physics*, (Saunders College, Philadelphia, 1976).

[4] K. S. Novoselov, A. K. Geim, S. V. Morozov, D. Jiang, Y. Zhang, S. V. Dubonos, I. V. Grigorieva, and A. A. Firsov, Science **306**, 666 (2004).

[5] L. Wang, I. Meric, P. Huang, Q. Gao, Y. Gao, H. Tran, T. Taniguchi, K. Watanabe, L. Campos, D. Muller *et al.*, Science **342**, 614 (2013).

[6] A. M. Morales and C. M. Lieber, Science **279**, 208 (1998).

[7] J. Hu, T. W. Odom, and C. M. Lieber, Acc. Chem. Res. **32**, 435 (1999).

[8] P. Michler, *Single Quantum Dots: Fundamentals, Applications and New Concepts*, (Springer, Germany, 2003).

[9] L. Fan, J. Wang, L. T. Varghese, H. Shen, B. Niu, Y. Xuan, A. M. Weiner, and M. Qi, Science **335**, 447 (2012).

[10] W. U. Huynh, J. J. Dittmer, and A. P. Alivisatos, Science **295**, 2425 (2002).

[11] T. Y. Fan and R. L. Byer, IEEE J. Quantum Electron. **24**, 895 (1988).

[12] P. A. Franken, A. E. Hill, C. W. Peters, and G. Weinreich, Phys. Rev. Lett. **7**, 118 (1961).

[13] G. R. Meredith, J. VanDusen, and D. J. Williams, Macromolecules **15**, 1385 (1982).

[14] W. Loh, S. Yegnanarayanan, R. J. Ram, and P. W. Juodawlkis, Sci. Rep. **4**, 3613 (2014).

[15] E. Kane, J. Phys. Chem. Solids **1**, 82 (1956).

[16] F. Bonabi and B. Bahrami, Mat. Sci. Semicon. Proc. **27**, 335 (2014).

[17] L. Pavesi and R. Turan, *Silicon Nanocrystals: Fundamentals, Synthesis and Applications*, (Wiley-VCH, 2010).

[18] J. H. Davies, *The Physics of Low-dimensional Semiconductors: An Introduction*, (Cambridge University Press, the United States of America, 1998).

[19] J. L. Bredas, C. Adant, P. Tackx, A. Persoons, and B. M. Pierce, Chem. Rev. **94**, 243 (1994).

[20] S. Eisler, A. D. Slepkov, E. Elliott, T. Luu, R. McDonald, F. A. Hegmann, and R. R. Tykwinski, J. Am. Chem. Soc. **127**, 2666 (2005).

[21] R. Saito, G. Dresselhaus, and M. Dresselhaus, *Physical Properties of Carbon Nanotubes*, (Imperial College Press, 1998).

[22] K. Hata, D. N. Futaba, K. Mizuno, T. Namai, M. Yumura, and S. Iijima, Science **306**, 1362 (2004).

[23] T. W. Ebbesen and P. M. Ajayan, Nature **358**, 220 (1992).

[24] X. Zhao, Y. Ando, Y. Liu, M. Jinno, and T. Suzuki, Phys. Rev. Lett. **90**, 187401 (2003).

[25] L. Shi, P. Rohringer, K. Suenaga, Y. Niimi, J. Kotakoski, J. C. Meyer, H. Peterlik, M. Wanko, S. Cahangirov, A. Rubio *et al.*, Nat. Mater. **15**, 634 (2016).

[26] L. Jiao, L. Zhang, X. Wang, G. Diankov, and H. Dai, Nature **458**, 877 (2009).

[27] D. Kosynkin, A. Higginbotham, A. Sinitskii, J. Lomeda, A. Dimiev, B. Price, and J. Tour, Nature **458**, 872 (2009).

[28] L. Tapasztó, G. Dobrik, P. Lambin, and L. P. Biró, Nat. Nanotechnol. **3**, 397 (2008).

[29] J. Cai, P. Ruffieux, R. Jaafar, M. Bieri, T. Braun, S. Blankenburg, M. Muoth, A. P. Seitsonen, M. Saleh, X. Feng, K. Müllen, and R. Fasel, Nature **466**, 470 (2010).

[30] P. Hohenberg and W. Kohn, Phys. Rev. **136**, B864 (1964).

[31] J. P. Perdew, Int. J. Quantum Chem. **28**, 497 (1985).

[32] L. Hedin, Phys. Rev. **139**, A796 (1965).

[33] M. S. Hybertsen and S. G. Louie, Phys. Rev. B **34**, 5390 (1986).

[34] F. Aryasetiawan and O. Gunnarsson, Rep. Prog. Phys. **61**, 237 (1998).

[35] F. Hüser, T. Olsen, and K. S. Thygesen, Phys. Rev. B **87**, 235132 (2013).

[36] J. L. Bredas, R. R. Chance, R. H. Baughman, and R. Silbey, J. Chem. Phys. **76**, 3673 (1982).

[37] Z. Zhang and C. M. Lieber, Appl. Phys. Lett. **62**, 2792 (1993).

[38] M. Ge and K. Sattler, Science **260**, 515 (1993).

[39] M. Ge and K. Sattler, Appl. Phys. Lett. **65**, 2284 (1994).

[40] C. H. Olk and J. P. Heremans, J. Mater. Res. **9**, 259 (1994).

[41] T. W. Odom, J.-L. Huang, P. Kim, and C. M. Lieber, Nature **391**, 62 (1998).

[42] J. W. Mintmire, B. I. Dunlap, and C. T. White, Phys. Rev. Lett. **68**, 631 (1992).

[43] N. Hamada, S.-i. Sawada, and A. Oshiyama, Phys. Rev. Lett. **68**, 1579 (1992).

[44] R. Saito, M. Fujita, G. Dresselhaus, and M. S. Dresselhaus, Appl. Phys. Lett. **60**, 2204 (1992).

[45] L. Shi, P. Rohringer, M. Wanko, A. Rubio, S. Waßerroth, S. Reich, S. Cambré, W. Wenseleers, P. Ayala, and T. Pichler, Phys. Rev. Mater. **1**, 075601 (2017).

[46] L. Brey and H. A. Fertig, Phys. Rev. B **73**, 235411 (2006).

[47] H. Zheng, Z. F. Wang, T. Luo, Q. W. Shi, and J. Chen, Phys. Rev. B **75**, 165414 (2007).

[48] Y.-W. Son, M. L. Cohen, and S. G. Louie, Phys. Rev. Lett. **97**, 216803 (2006).

[49] V. Barone, O. Hod, and G. E. Scuseria, Nano Lett. **6**, 2748 (2006).

[50] K. A. Ritter and J. W. Lyding, Nat. Mater. **8**, 235, article (2009).

[51] M. Y. Han, B. Özyilmaz, Y. Zhang, and P. Kim, Phys. Rev. Lett. **98**, 206805 (2007).

[52] R. L. E. T. A. Skotheim and J. R. Reynolds, *Handbook of Conducting polymers*, (MARCEL DEKKER, INC, New York, 1998).

[53] H. Hsu and L. E. Reichl, Phys. Rev. B **76**, 045418 (2007).

[54] W. Liao, G. Zhou, and F. Xi, J. Appl. Phys. **104**, 126105 (2008).

[55] K.-i. Sasaki, K. Kato, Y. Tokura, K. Oguri, and T. Sogawa, Phys. Rev. B **84**, 085458 (2011).

[56] M. Wang, Y. C. Wang, H. X. Zhao, and S. X. Song, RSC Adv. **5**, 68722 (2015).

[57] X. Zhu and M. Wang, RSC Adv. **6**, 11786 (2016).

[58] K. O. Wedel, N. A. Mortensen, K. S. Thygesen, and M. Wubs, Phys. Rev. B **99**, 045411 (2019).

[59] K. F. Mak, M. Y. Sfeir, Y. Wu, C. H. Lui, J. A. Misewich, and T. F. Heinz, Phys. Rev. Lett. **101**, 196405 (2008).

[60] F. Hipolito, T. G. Pedersen, and V. M. Pereira, Phys. Rev. B **94**, 045434 (2016).

[61] S. A. Mikhailov, Phys. Rev. B **90**, 241301 (2014).

[62] E. Hendry, P. J. Hale, J. Moger, A. K. Savchenko, and S. A. Mikhailov, Phys. Rev. Lett. **105**, 097401 (2010).

[63] G. Y. Guo, K. C. Chu, D.-s. Wang, and C.-g. Duan, Phys. Rev. B **69**, 205416 (2004).

[64] J. D. Correa, A. J. R. da Silva, and M. Pacheco, J. Phys. Condens. Matter **22**, 275503 (2010).

[65] H. Kataura, Y. Kumazawa, Y. Maniwa, I. Umezu, S. Suzuki, Y. Ohtsuka, and Y. Achiba, Synth. Met. **103**, 2555 (1999).

[66] R. S. Knox, *Introduction to Exciton Physics*, (Springer US, Boston, MA, 1983).

[67] S. Albrecht, L. Reining, R. Del Sole, and G. Onida, Phys. Rev. Lett. **80**, 4510 (1998).

[68] M. Ichida, S. Mizuno, Y. Saito, H. Kataura, Y. Achiba, and A. Nakamura, Phys. Rev. B **65**, 241407 (2002).

[69] T. G. Pedersen, Phys. Rev. B **67**, 073401 (2003).

[70] T. G. Pedersen, Carbon **42**, 1007 (2004).

[71] G. Dukovic, F. Wang, D. Song, M. Y. Sfeir, T. F. Heinz, and L. E. Brus, Nano Lett. **5**, 2314 (2005).

[72] J. Jiang, R. Saito, G. G. Samsonidze, A. Jorio, S. G. Chou, G. Dresselhaus, and M. S. Dresselhaus, Phys. Rev. B **75**, 035407 (2007).

[73] Y. Miyauchi, R. Saito, K. Sato, Y. Ohno, S. Iwasaki, T. Mizutani, J. Jiang, and S. Maruyama, Chem. Phys. Lett. **442**, 394 (2007).

[74] J. Deslippe, M. Dipoppa, D. Prendergast, M. V. O. Moutinho, R. B. Capaz, and S. G. Louie, Nano Lett. **9**, 1330 (2009).

[75] T. Ando, Physica E Low Dimens. Syst. Nanostruct. **43**, 798 (2011).

[76] F. Wang, G. Dukovic, L. E. Brus, and T. F. Heinz, Science **308**, 838 (2005).

[77] N. Cade, Chem. Phys. Lett. **53**, 45 (1978).

[78] E. Mostaani, B. Monserrat, N. D. Drummond, and C. J. Lambert, Phys. Chem. Chem. Phys. **18**, 14810 (2016).

[79] T. G. Pedersen, Phys. Rev. B **69**, 075207 (2004).

[80] J.-W. Van der Horst, P. Bobbert, M. Michels, and H. Bässler, J. Chem. Phys. **114**, 6950 (2001).

[81] M. Rohlfing and S. G. Louie, Phys. Rev. B **62**, 4927 (2000).

[82] A. Pospischil, M. Humer, M. M. Furchi, D. Bachmann, R. Guider, T. Fromherz, and T. Mueller, Nat. Photonics **7**, 892 (2013).

[83] M. Liu, X. Yin, E. Ulin-Avila, B. Geng, T. Zentgraf, L. Ju, F. Wang, and X. Zhang, Nature **474**, 64 (2011).

[84] S.-W. Chang, J. Hazra, M. Amer, R. Kapadia, and S. B. Cronin, ACS Nano **9**, 11551 (2015).

[85] W. Franz, Z. Naturforsch. A **13**, 484 (1958).

[86] L. Keldysh, Sov. Phys. JETP **34**, 788 (1958).

[87] D. A. B. Miller, D. S. Chemla, and S. Schmitt-Rink, Phys. Rev. B **33**, 6976 (1986).

[88] T. G. Pedersen and T. B. Lynge, Phys. Rev. B **65**, 085201 (2002).

[89] C. H. Lee, R. K. Chang, and N. Bloembergen, Phys. Rev. Lett. **18**, 167 (1967).

[90] M. Nakano, K. Yamaguchi, Y. Matsuzaki, K. Tanaka, and T. Yamabe, Chem. phys. lett. **233**, 411 (1995).

[91] V. Jašinskas, M. Gedvilas, G. Račiukaitis, and V. Gulbinas, Opt. Lett. **41**, 2759 (2016).

[92] A. Cavallini, L. Polenta, M. Rossi, T. Stoica, R. Calarco, R. Meijers, T. Richter, and H. Lüth, Nano lett. **7**, 2166 (2007).

[93] D. Li, J. Zhang, Q. Zhang, and Q. Xiong, Nano lett. **12**, 2993 (2012).

[94] G. Weiser, Phys. Rev. B **45**, 14076 (1992).

[95] A. Horvath, G. Weiser, C. Lapersonne-Meyer, M. Schott, and S. Spagnoli, Phys. Rev. B **53**, 13507 (1996).

[96] G. Weiser, L. Legrand, T. Barisien, A. Al Choueiry, M. Schott, and S. Dutremez, Phys. Rev. B **81**, 125209 (2010).

[97] K. Yamamoto, T. Kamata, S. Iwai, S. Kazaoui, N. Minami, F. Mizukami, K. Misawa, T. Ohta, and T. Kobayashi, Chem. Phys. Lett. **302**, 609 (1999).

[98] M.-H. Ham, B.-S. Kong, W.-J. Kim, H.-T. Jung, and M. S. Strano, Phys. Rev. Lett. **102**, 047402 (2009).

[99] R.-B. Chen and Y.-T. Lu, Phys. Lett. A **264**, 417 (2000).

[100] S. Hughes and D. Citrin, Phys. Rev. lett. **84**, 4228 (2000).

[101] T. G. Pedersen and T. B. Lynge, J. Phys.: Cond. Mat. **15**, 3813 (2003).

[102] C. Xia and H. N. Spector, J. Appl. Phys. **105**, 084313 (2009).

[103] C. Xia, S. Wei, and H. N. Spector, Physica E **42**, 2065 (2010).

[104] M. Sakai and M. Yamaguchi, Physica E **21**, 367 (2004).

[105] H. Raza and E. C. Kan, Phys. Rev. B **77**, 245434 (2008).

[106] W. Apel, G. Pal, and L. Schweitzer, Phys. Rev. B **83**, 125431 (2011).

[107] K. Gundra and A. Shukla, Phys. Rev. B **83**, 075413 (2011).

[108] S. Bala Kumar, T. Fujita, and G. Liang, J. Appl. Phys. **109**, 073704 (2011).

[109] H. C. Chung, C. P. Chang, C. Y. Lin, and M. F. Lin, Phys. Chem. Chem. Phys. **18**, 7573 (2016).

[110] F. Afshari and M. Ghaffarian, Physica. E: Low dimens. Syst. Nanostruct. **89**, 86 (2017).

[111] Y. C. Huang, C. P. Chang, and M. F. Lin, J. Appl. Phys. **104**, 103714 (2008).

[112] S. Bala Kumar and J. Guo, Appl. Phys. Lett. **98**, 263105 (2011).

[113] S. Bala Kumar and J. Guo, J. Appl. Phys. **110**, 044309 (2011).

[114] F. L. Shyu, Physica B: Condens. Matter **452**, 7 (2014).

[115] R. Alaei and M. H. Sheikhi, Fuller. Nanotub. Car. N. **21**, 183 (2013).

[116] V. Perebeinos and P. Avouris, Nano Lett. **7**, 609 (2007).

[117] H. Garcia, Phys. Rev. B **74**, 035212 (2006).

[118] C. Xia and H. N. Spector, J. Appl. Phys. **106**, 124302 (2009).

[119] J. Heflin, Y. Cai, and A. Garito, J. Opt. Soc. Am. B **8**, 2132 (1991).

[120] S. Reich, J. Maultzsch, C. Thomsen, and P. Ordejón, Phys. Rev. B **66**, 035412 (2002).

[121] R. W. Boyd, (Academic Press, San Diego, USA, 1992).

[122] G. Strinati, Riv. Nuovo Cimento (1978-1999) **11**, 1 (1988).

[123] C. D. Spataru, S. Ismail-Beigi, L. X. Benedict, and S. G. Louie, Phys. Rev. Lett. **92**, 077402 (2004).

[124] V. Perebeinos, J. Tersoff, and P. Avouris, Phys. Rev. Lett. **92**, 257402 (2004).

[125] E. Chang, G. Bussi, A. Ruini, and E. Molinari, Phys. Rev. Lett. **92**, 196401 (2004).

[126] J. Maultzsch, R. Pomraenke, S. Reich, E. Chang, D. Prezzi, A. Ruini, E. Molinari, M. Strano, C. Thomsen, and C. Lienau, Phys. Rev. B **72**, 241402 (2005).

[127] Y.-Z. Ma, L. Valkunas, S. M. Bachilo, and G. R. Fleming, J. Phys. Chem. B **109**, 15671 (2005).

[128] H. Liu, S. Schumacher, and T. Meier, Phys. Rev. B **89**, 155407 (2014).

[129] Q. Bao and K. P. Loh, ACS Nano **6**, 3677 (2012).

[130] Y. Zhou and M. W. Wu, Phys. Rev. B **83**, 245436 (2011).

[131] H. K. Kelardeh, V. Apalkov, and M. I. Stockman, Phys. Rev. B **90**, 085313 (2014).

[132] W. Kohn and L. J. Sham, Phys. Rev. **140**, A1133 (1965).

[133] X. Gonze, B. Amadon, P. Anglade, J. Beuken, F. Bottin, P. Boulanger, F. Bruneval, D. Caliste, R. Caracas, M. Cote, T. Deutsch, L. Genovese, P. Ghosez, M. Giantomassi, S. Goedecker, D. Hamann, P. Hermet, F. Jollet, G. Jomard, S. Leroux, M. Mancini, S. Mazevet, M. Oliveira, G. Onida, Y. Pouillon, T. Rangel, G. M. Rignanese, D. Sangalli, R. Shaltaf, M. Torrent, M. Verstraete, G. Zerah, and J. Zwanziger, Comput. Phys. Commun. **180**, 2582 (2009).

[134] M. Balkanski and R. F. Wallis, *Semiconductor Physics and Apllications*, (Oxford University Press, New York, 2007).

[135] T. G. Pedersen, *Electric, Optical and Magnetic Properties of Nanostructures*, (Aalborg University, 2018, url: http://homes.nano.aau.dk/tgp/).

[136] T. G. Pedersen, Phys. Rev. B **69**, 075207 (2004).

[137] D. Emin and C. F. Hart, Phys. Rev. B **36**, 7353 (1987).

[138] J. Wahlstrand and J. Sipe, Phys. Rev. B **82**, 075206 (2010).

[139] C. Aversa and J. E. Sipe, Phys. Rev. B **52**, 14636 (1995).

[140] J. K. Wahlstrand and J. E. Sipe, Phys. Rev. B **82**, 075206 (2010).

[141] X. Gonze, J.-M. Beuken, R. Caracas, F. Detraux, M. Fuchs, G.-M. Rignanese, L. Sindic, M. Verstraete, G. Zerah, F. Jollet *et al.*, Comput. Mater. Sci. **25**, 478 (2002).

[142] X. Gonze, B. Amadon, P.-M. Anglade, J.-M. Beuken, F. Bottin, P. Boulanger, F. Bruneval, D. Caliste, R. Caracas, M. Côté *et al.*, Compu. Phys. Commun. **180**, 2582 (2009).

[143] F. Bottin, S. Leroux, A. Knyazev, and G. Zérah, Comput. Mater. Sci. **42**, 329 (2008).

[144] M. Torrent, F. Jollet, F. Bottin, G. Zérah, and X. Gonze, Comput. Mater. Sci. **42**, 337 (2008).

[145] J. P. Perdew, K. Burke, and M. Ernzerhof, Phys. Rev. Lett. **77**, 3865 (1996).

[146] N. A. Lanzillo, N. Kharche, and S. K. Nayak, Sci. Rep. **4**, 3609 (2014).

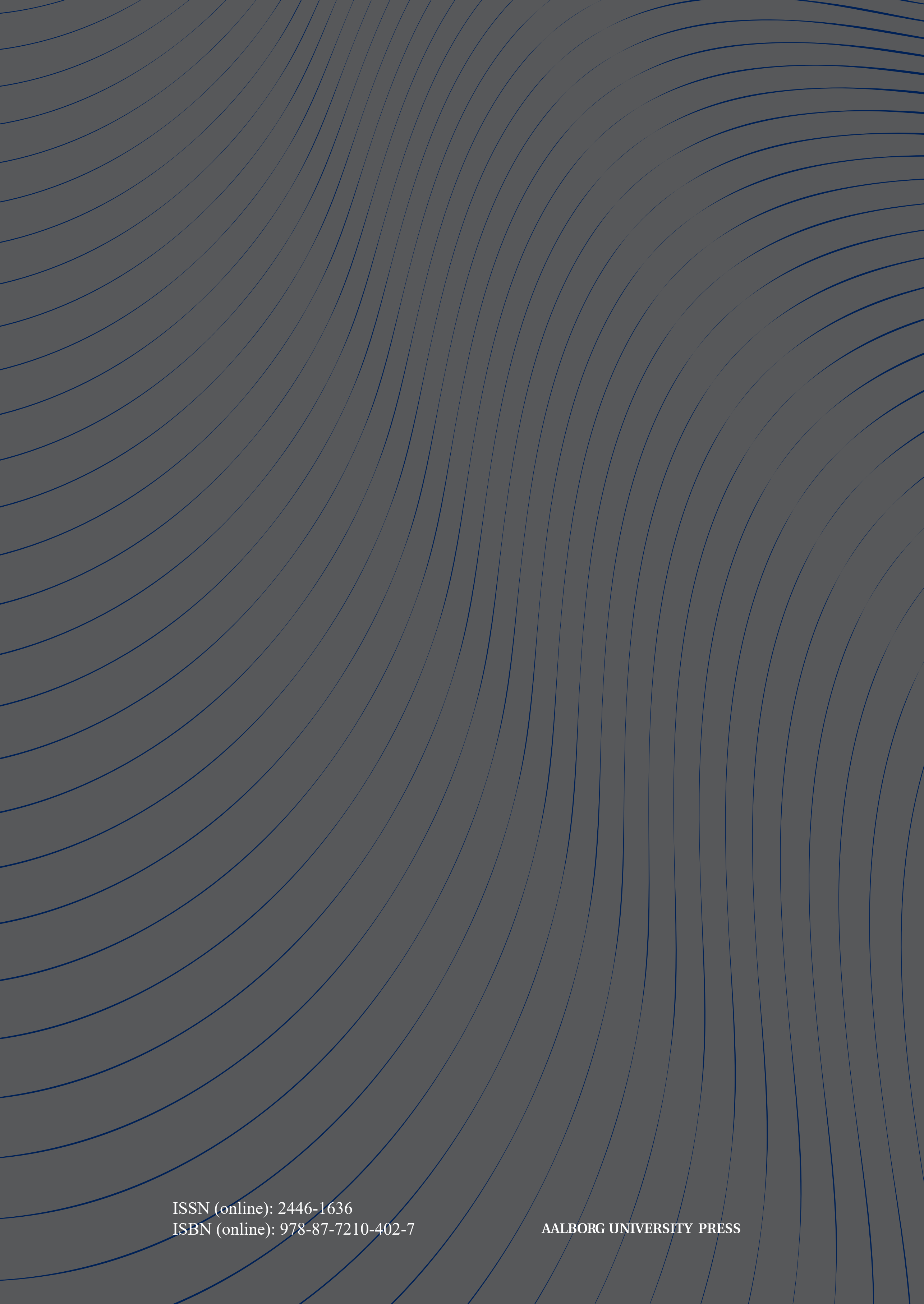

ISSN (online): 2446-1636
ISBN (online): 978-87-7210-402-7

AALBORG UNIVERSITY PRESS